Exergy-Based Ecological Network Analysis for Building and Community Energy Systems

Preprint · September 2023

DOI: 10.2139/ssrn.4578446

3 authors:

Kathryn Hinkelman
Pennsylvania State University
34 PUBLICATIONS **220** CITATIONS
SEE PROFILE

Saranya Anbarasu
Pennsylvania State University
15 PUBLICATIONS **12** CITATIONS
SEE PROFILE

Wangda Zuo
Pennsylvania State University
187 PUBLICATIONS **3,404** CITATIONS
SEE PROFILE

Exergy-based ecological network analysis for building and community energy systems

Kathryn Hinkelman[a], Saranya Anbarasu[a], Wangda Zuo[a,*]

[a]*Department of Architectural Engineering, Pennsylvania State University, University Park, 16802, PA, USA*

Abstract

Although buildings are transitioning towards complex, dynamic, and interconnected systems, traditional engineering metrics that dominate today don't capture several important whole-network properties. To address this, we adopt ecological network analysis (ENA), which has numerous successes for natural ecosystems and socio-technical systems but has yet to be applied for buildings. After translating ENA into comprehensive mathematical models for engineering applications, we demonstrate the novel ENA method with building and community energy systems. For the models to suit building energy systems, which have multiple energy types and non-negligible dynamics, we formulate ENA on an exergy basis, with dynamic flows and balances (i.e., time-varying storages). To demonstrate the proposed approach, we use ENA to redesign the heating and cooling systems for an office building and data center, coupling the buildings together via ambient-loop district energy. The models are implemented using the equation-based Modelica language. Results indicate that the ENA-guided redesign reduces the source energy by 15%. The energy consumed by the heating and cooling systems is reduced by 84% with negligible sacrifice to the thermal performance. Surprisingly, the redesign also reduced the exergy efficiency of the total system from 60% to 34% due to a greater decrease in exergy output relative to exergy input with low-exergy system designs. This indicates that ENA and other network approaches that classify system organization may outperform traditional efficiency-based metrics for building and community energy systems when whole-system perspectives are desired.

Keywords: district energy, dynamic systems, ecosystem biomimicry, exergy, graph theory, Modelica

*Corresponding author.
Email address: wangda.zuo@psu.edu (Wangda Zuo)

Nomenclature

Abbreviations

CHW	Chilled Water
CHWS/CHWR	Chilled Water Supply/Return
CW	Condenser Water
CWS/CWR	Condenser Water Supply/Return
DES	District Energy System
DW	District Water
ENA	Ecological Network Analysis
HVAC	Heating, Ventilation, and Air Conditioning
KPI	Key Performance Indicator
MBL	Modelica Buildings Library
MSL	Modelica Standard Library
PUE	Power Usage Effectiveness
RA	Return Air
SA	Supply Air
TCE	Tons of Coal Equivalent
VAV	Variable Air Volume
WB	Wetbulb
WSE	Waterside Economizer

Accents

$*$	Apparent
$\dot{\cdot}$	Flow rate

Subscripts

0	External/Initial
app	Approach
c	Internal flow/cycling
coo	Cooling
dat	Data center
dcs	Data center cooling system
equ	Electrical equipment
$extWal$	Exterior wall
hea	Heating
I	Energy-basis (1st law)
i, j, k	Indices
II	Exergy-basis (2nd law)
in	Inward
$intWal$	Interior wall
n	Nominal
off	Office
out	Outward
pip	Pipe
r	Direct
Rad	Radiation
ser	Servers
set	Setpoint
sit	Site
sou	Source
$tubSeg$	Borefield tube segment
unm	Unmet

Variables

α	Degree of system order
Γ	Heat capacity
$\mathbb{I}$	Origin set
$\mathbb{J}$	Destination set
Φ, ϕ	Reserve
Ψ	Total system throughput
$\dot{r}$	Through-flow
A, a	Ascendancy
C, c	Capacity
d	Dissipation/Destruction
f	Compartmental flow
FCI	Finn's cycling index
h	Specific enthalpy
n	Number of compartments
p	Pressure
Q	Heat
s	Specific entropy
T	Temperature
t	Time
V	Volume
W	Work
X	Exergy stored
y	External output
z	External input

1. Introduction

1.1. Motivation

To improve performance and comfort, buildings are becoming complex dynamical systems with physical and operational integration across multiple functional domains [1]. Meanwhile, highly

intermittent supply (e.g., solar and wind power) and increasing demand due to electrification of transportation and heating, among other factors [2], are causing electric grids to evolve into fully distributed networks that are intelligent, responsive, dynamic, flexible, and adaptive [3]. Spanning multiple domains, there are numerous examples of cross-sectoral integration of physical and control systems being implemented today, including *building-to-grid* [4], *vehicle-to-grid* [5], and *power-to-X* [6]. All together, these transitions create a situation where individual and coupled effects of multiple system dynamics are increasingly relevant to design and operation.

Despite buildings becoming more complex, dynamic, and interconnected, evaluation metrics that dominate today are most often independent of network structure and flows. This is demonstrated in Figure 1. Traditional engineering metrics typically focus on system inputs, outputs, and losses of various types (e.g., site/source energy, water, costs, carbon emissions) at various levels (e.g., single equipment, subsystems, complete systems), which are depicted with black arrows in Figure 1. These traditional metrics include ratios of outputs/inputs (i.e., efficiency), combinations of multiple inputs/outputs (e.g., multi-objective optimization), and rate forms (e.g., peak power vs. total energy). From this perspective, systems A and B produce the same results. However, the networks are highly different. System A is a linear, one-directional network, while system B involves greater complexity (i.e., more cycling, more redundant pathways). To design resilient, healthy, zero-carbon energy systems for buildings, we need new approaches that quantify the complexity of networked systems (i.e., the gray components of Figure 1, exhibiting dependence on network structure and flows).

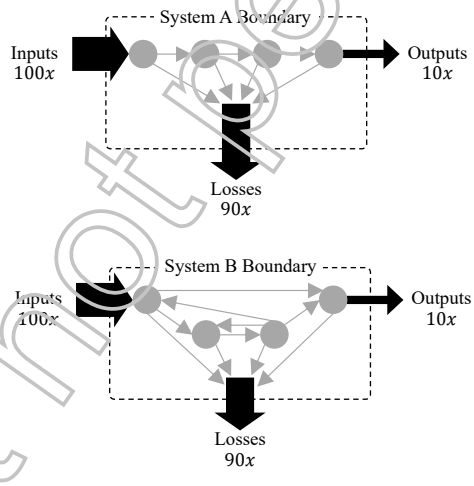

Figure 1: Comparison between two theoretical systems A and B with system boundaries in dashed black lines, where inputs/outputs/losses (black arrows) are independent of network structure and flows (gray circles and arrows).

To solve this challenge, there is an opportunity to adopt ecological network analysis (ENA) for building applications. In brief, ENA is a graph-theoretic whole-systems analysis method that quantifies the *organization* of networked systems to illuminate characteristics for *sustainable growth and development* [7]. While the majority of ENA applications focus on studying food web ecosystems [8], engineering researchers have also adopted ENA for industrial systems [9], manufacturing supply chains [10], and cyber-physical power systems [11]. Although ENA has been highly effective outside of the building's domain, it remains unclear if ENA is suitable for building applications. As such, the purpose of this study is to develop and evaluate ENA for building energy systems,

which are complex dynamic engineering systems with multiple energy types. For heterogeneous energy systems, we introduce an *exergy-based* approach to ENA literature, and demonstrate our novel approach for integrated thermofluid-electrical systems in the built environment.

1.2. Literature Review

In ENA, one analyzes exchanges of energy and/or materials through trophic levels of food webs to understand relationships between biodiversity and ecological stability [12]. Mathematically, ENA originates from information theory, graph theory, economic input-output analysis, and thermodynamics, which is detailed in one of the seminal works by [7]. Figure 2 depicts the standard ENA process from the physical ecosystem to the matrix model. The major steps are as follows. First, the ecological food web is mapped to a weighted directed network graph (i.e., weighted digraph) that represents the transfers of energy (or matter) with respect to participating agents (animals, plants, microorganisms, etc.) as f_{ij}, where i is the source and j is the sink. In Figure 2a, each agent represents a *compartment*, and this example system involves $n = 5$ compartments. Compartment dissipations (i.e., losses) are represented as electrical ground symbols. With graph theory, the weighted digraph can simply be represented as a matrix with elements f_{ij}, as shown in Figure 2b. Here, index 0 represents the inputs or outputs with respect to the external environment, and index $n+1$ represents the dissipations. From the non-symmetric matrix representation in Figure 2b, ENA applies several whole-system metrics to quantify the organization of the network. These metrics will be discussed further in section 3.3

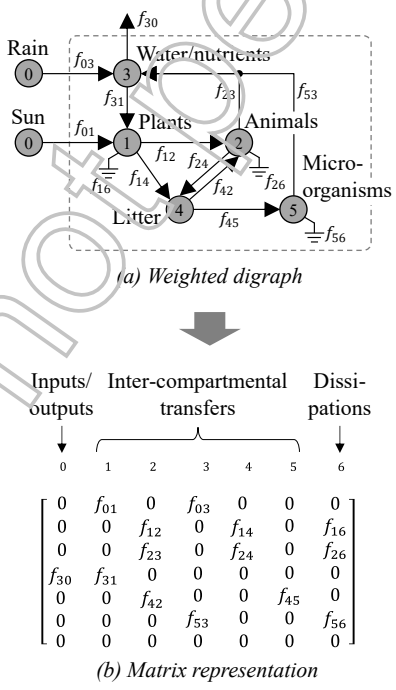

Figure 2. A typical ENA process from the (a) network digraph to (b) matrix representation.

Application topics have spanned a wide range of biological, technical, social, and economic applications, all of which represent complex, interconnected *systems of systems*. Among previous literature, analysis of food web ecosystems have dominated, while energy and urban metabolism

and wetland water systems have also benefited from ENA [8]. While a complete review of literature on ENA in biological applications is out of the scope of this paper, well-documented exemplary works include [13] and [14]. For these studies, most have adopted *conserved, steady-state* system models with *homogeneous* flows. In other words, all f_{ij} in Figure 2c are *constants* (steady) of the same energy/material type (homogeneous), and $\sum_{j=0}^{n+1}(f_{ji} - f_{ij}) = 0,\ \forall\ i \in 1...n$ (conserved). Several software tools are available for these systems, including enaR [15], ECOPATH II [16], and the MATLAB function NEA [17].

Among biological applications, some researchers have developed ENA approaches and metrics for dynamic models. Some works treat temporal dynamics as "a time series of network snapshots" [18] by repeating steady-state analyses on seasonal or annual bases. Others have adopted Lagrangian agent-based techniques with network particle tracking [19, 20]. Some dynamic ENA formulation with state-space representations are available, which are more practical and less computationally expensive for complex system models. [21] developed a closed-form formulation for nonlinear systems. Extending this early work, [12] developed comprehensive model formulations for dynamic ENA with system and subsystem partitioning methodologies based on a decomposition principle [22]. While most of the above studies leveraged proprietary software, Stella [23] is a popular systems thinking tool with simple dynamic modeling capabilities that has been previous adopted for ENA [13].

Beyond the original biological domains, ENA has also been used to design engineering and socio-economical systems. Because these socio-technical applications of ENA are central to this paper, we reviewed these studies in detail and summarized our findings in Table 4 of the Appendix. Across 33 studies, the far majority were steady-state analyses with a time step of one year. Modeling homogeneous systems, past use cases included networks of carbon dioxide emissions [24], carpet recycling [9], embodied energy [25], and water [26], among others. On the other hand, heterogeneous system models included cyber-physical power systems [11], energy [27], energy-water [28], and urban-industrial systems [29]. Researchers adopted several methods when combining heterogeneous flow within ENA, as indicated in the *ENA unit(s)* column of Table 4. For example, [11] took the product of all flows, resulting in units of *power-packets*. Some other studies summed all flows, which resulted in inconsistent units, such as with [30] (*energy+volume*) and [29] (*energy+mass*). With heterogeneous energy systems, several studies normalized all energy types using the energy-based tons of coal equivalent (TCE) conversion [31, 32, 27], while [33] took an unweighted sum on an energy-basis. For software tools, MatLab was the most commonly reported tool [9, 10, 11, 34, 26, 35], while [36] adopted AnyLogic, [27] used MatLab and Python, [37] used MatLab and Julia, and[38] used PowerWorld.

Among all non-biological ENA studies in Table 4, only one implemented dynamic ENA. [36] used AnyLogic [39] to develop and simulate a dynamic system model for a forestry industry case study. In this study, the time step was fixed at 1 week; this was the shortest time step of all non-biological ENA studies reviewed herein. AnyLogic [39] can model system dynamics similar to Stella [23], while it also supports agent-based, discrete event, and multi-method modeling. Numerical solvers for both Stella and AnyLogic include multiple explicit methods with fixed time steps, such as Euler and RK4 [23, 39].

In brief, the majority studies in biological and engineering applications adopt steady ENA. Several biological studies developed dynamic ENA implementations that are suitable for ecological studies, but only [36] applied dynamic ENA for a non-biological application (forestry industry). To the authors' knowledge, no studies have yet to apply ENA for building applications, including

building and community energy systems, and no studies have applied dynamic ENA for energy in engineering systems.

1.3. Contributions

To enable ENA for complex dynamic systems with heterogeneous flows, which are common in real-world engineering systems, two critical challenges need to be addressed. First, we need a comprehensive approach for ENA that can solve large and sparse systems of differential algebraic equations that often contain discontinuous functions, nonlinear behavior, and stiff systems, which are common of building and community energy systems. To capture important system dynamics, the model also requires fine time resolution (i.e., microseconds to hours), while the simulator needs to accommodate *stiff* problems with both fast and slow dynamics. The existing ENA software (i.e., Stella, AnyLogic) cannot solve these complex problems, and existing ENA formulations have yet to demonstrate these capabilities for real-world applications, to our knowledge. Second, we need a method to aggregate multiple energy types of dissimilar qualities that change with time. The approaches used to date, such as TCE, are practical for carbon-based fuels, but they cannot capture the variability of modern thermofluid, mechanical, and chemical energy types, which are common in building and community energy systems.

By addressing these gaps, this work provides a pathway for applying ENA for numerous complex system models across the engineering sciences and real-world practices. Further, ENA has the potential to improve building and community analysis methods by adding whole-network information beyond the capabilities of the metrics used today (as presented with Figure 1). To meet these aims, four intermediate objectives will be pursued: (1) provide a comprehensive mathematical formulation for ENA of dynamic, heterogeneous systems that aggregates dissimilar energy flows based on exergy; (2) implement our exergy-based ENA formulation in a multi-domain language that can support both causal (ENA structure and controls) and acausal modeling (physical systems) and efficiently simulate stiff, hybrid differential algebraic systems of equations with discontinuities and nonlinearities; (3) demonstrate ENA for a case study for building and community energy systems with electrical and thermofluid components; and (4) determine if and how ENA may augment traditional energy- and efficiency-based analysis methods for future studies.

The rest of the paper is organized as follows. In section 2, we present our methodology that is tailored for ENA for complex dynamical engineering systems. Section 3 presents our comprehensive mathematical formulation, while section 4 details the case study systems and model implementations. For this work, the equation-based object-oriented Modelica language [40] is selected to implement our novel ENA approach, which has yet to be used for ENA and is capable of solving the problems we require. The baseline case study system is a site with separate data center and office buildings. Following the presented methodology, these systems are iteratively redesigned, coupling the heating and cooling systems together via an ambient-loop district energy system (DES), before further modifying controls and equipment. The case study results are presented in section 5. Finally, sections 6 and 7 discuss the findings, propose future work, and summarize broader impacts.

2. Methodology

This work addresses the need for new whole-network analysis methods for building and community energy systems. To adopt ENA from biological sciences for engineering applications, we follow standardized methods for biomimetics [41]. Biomimetics aims to solve "practical problems

through the functional analysis of *biological systems*, their *abstraction* into *models*, and the transfer into and application of these models to the solution" [41]. Models of sustainable natural food web ecosystems are measured and evaluated with ENA in several previous works [15]. To translate these models for building and community energy systems, this work adopts ENA for this new application domain and evaluates the performance with simulation-based case studies. Because of the novelty of biomimetics and ENA for the building simulation community, we focus on those aspects of the research. In contrast, it is worth noting that building energy modeling and the development of new HVAC technologies are not the focus of this paper. However, readers can find more information regarding system modeling and simulation in [42] and HVAC design in [43].

As shown in Figure 3, this work follows a biomimetics approach tailed for simulation-based assessment of novel engineering system technologies. Specifically, this work adopts a *technology pull* approach to biomimicry with focus on understanding biological principles, abstracting the principles from the biological model, checking for technical feasibility, and improving the product. Tailored for building and community energy simulations, the corresponding four stages of our methodology are (1) prepare the problem, (2) translate principles, (3) run experiments, and (4) evaluate systems. The first two stages of ISO 18458 – technical problem definition and search for analogies in biology – were the focus of our previous review publication [44]. Sections 2.1-2.4 present the details for each of the four main steps employed in this work.

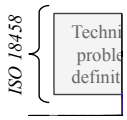

Figure 3: Methodology for ENA-based design and performance evaluation with respect to the technology pull approach from ISO 18458 [41].

2.1. Prepare the Problem

To prepare the problem and *understand the principles* both in the engineering and biological systems, the initial steps focus on defining the engineering system and original ENA formulation. Regarding the engineering system, we first define the scientific experiment and decide what measurable question the models should answer. The goal is not to have the models represent all aspects of the real system, but only the features that are necessary to answer the problem's research questions in measurable, meaningful ways. For example, this case study involves district-scale energy systems during normal operating conditions, including minutely to hourly transient thermal and electrical behavior, which greatly affect energy performance. This foundational understanding is critical to ensure the model captures the correct dynamics for the intended assessment.

Similarly, understanding the physical foundation of the original biological model – in this case, the original ENA formulation – helps ensure that the model is abstracted correctly to the engineering application. In particular, care must be taken to understand the language used to communicate requirements, methodologies, and impacts. This includes the assumptions and limitations of the biological models, which become increasingly important in biomimetics research because the models often are extended beyond their originally intended domain. Two effective strategies to address these challenges include comprehensive literature review and consulting experts from the original biological field to validate comprehension.

After understanding the engineering system, we then develop the system model and directed graph (i.e., digraph) for ENA. To form the digraph, the system is first compartmentalized based on the study objective and data availability. For example, a district energy simulation may lump the HVAC system for each building as one compartment, while a single building simulation may represent each equipment as one compartment. Then, edges are then determined based on physical connections between compartments and with external sources/sinks. This completes the unweighted digraph. Weights (edges and compartmental storages) are determined in the next step.

2.2. Translate Principles

This step abstracts the biological principles and translates those principles for engineering applications. To adopt ENA for dynamic engineering systems, the mathematics need to be modified for the targeted physics. Section 3 presents the results of this process. Further, implementing the ENA mathematical models so that they can be solved efficiently with numerical solvers requires additional attention. For example, several ENA metrics – such as ascendancy Eq. (8) – involve logarithmic functions and divisions. For initialization or instances where exergy flows are zero (i.e., solar photovoltaic power output during the middle of the night), special considerations are required to avoid division by zero errors. Further, all solutions need to maintain non-negative inputs for logarithm functions, a challenge also encountered by [37]. To address these challenges, we implement a smooth max() function that provides a once continuously differentiable approximation near zero. This results in ENA metrics where $\lim_{x\to 0}[f_1(x)/f_2(x)] = 1/1$. While this introduces small calculation errors, the impact on results are negligible, and the benefit of increasing the likelihood that the problem can be solved numerically is great.

Beyond the mathematical formulations of the engineering system and ENA, there are additional implementation considerations for modeling and simulating these complex systems. On the modeling side, these problems involve hybrid (i.e., both discrete and continuous) differential algebraic equations. Further, support of both causal and acausal modeling aids model development; this allows system physics to be represented in standard equation forms while controls and network structure can be structured with $A \to B$ causalities. The modeling support of multiple engineering domains can allow integrated heterogeneous systems to be represented within one simulation environment. On the simulation side, the numerical solver needs to accommodate *stiff* problems with both fast and slow dynamics, which are typical of integrated energy systems (i.e., thermofluid and electrical, gas and electrical, etc.).

To address these challenges, this paper adopts Modelica [40]. Modelica is an equation-based and object-oriented modeling language for complex, dynamic, integrated systems. While Modelica is new for ENA, it is well established for the building simulation community, thus making it an appropriate choice. There are several reasons why Modelica is suitable for the target problems, including the support of both causal and acausal modeling and the availability of several numerical solvers, many of which support stiff and sparse systems of equations with discontinuities and

nonlinearities. Examples of Modelica-based modeling related to this work are available in the Modelica Buildings Library [45] and the Biomimetic Integrated Community Energy and Power Systems (BICEPS) Library [46].

2.3. Run Experiments

To check the feasibility of the system and ENA formulation, we ran annual simulation experiments. Simulations ran in Dymola 2022 with the CVODE solver[47] and a simulation tolerance of 10^{-6}. In our experience of adopting CVODE in Dymola, it typically simulates thermofluid systems quickly and robustly, but other solvers such as DASSL and RADAU are often suitable. Further, because these systems of equations were large and sparse, we utilized the sparse solving capabilities of CVODE to improve the computing efficiency (via Dymola flag *SparseActivate* with two cores).

As an example, the problem formulation and computing times for these four case studies were as follows. In the original models, the four systems contained 5467-9731 nontrivial equations. After Dymola's pre-processing algorithms [48], the models contained 220-335 continuous time states, 1-2 linear systems of equations (2-3 iteration variables each), 6-12 nonlinear systems of equations (1-3 iteration variables each). To note, before Dymola's pre-processing algorithms, these system models contained 4-24 linear systems (3-28 variables each) and 6-13 nonlinear systems (1-53 variables each). On a laptop computer (Windows OS, 36GB RAM, 2.20GHz Intel® Core™ i7-8750H CPU), each annual simulation took from 86 seconds (baseline) to 325 seconds (redesign 2).

Before using the simulation results, a critical step is to validate the system performance and network flows. Regarding system performance, this includes both the physical system and controls. Validating the physical system includes checking the pressure drops and flow rates (fluid dynamics), temperatures and enthalpies (heat transfer), and equipment performance with respect to design parameters. For controls, these models implement several PI controllers for pumps and equipment. These controller gains requiring tuning for stable performance and often require re-tuning for each system configuration. Lastly, in terms of network flows, we know from thermodynamics that energy is always conserved and exergy is always destroyed; as such, if exergy is being generated within compartments at any time, then the model physics need to be corrected.

2.4. Evaluate Systems

With the simulation results validated, system performance can be assessed across several key performance indicators (KPIs). To determine the suitability of ENA for integrated building energy systems, we evaluate both traditional and ENA-based KPIs (summarized in Table 1). Because traditional KPIs are not the focus of this work but used for comparative evaluation, their equations are provided in the Appendix. Several efficiency-based metrics are employed, including the power usage effectiveness (PUE), site and source energy efficiency ($\eta_{I,sit}$ and $\eta_{I,sou}$, respectively), and source exergy efficiency ($\eta_{II,sou}$). For heating and cooling systems, traditional metrics also include the total number of unmet hours of cooling and heating (t_{unm}); the modeled temperatures at various locations (e.g., office zone, data center servers, DES pipes, borefield); and the source energy use (E_{sou}). In the office zone, we target a maximum of 300 unmet hours per Standard 90.1 [49].

Based on the ENA-based KPIs, several design iterations are performed. The objective is to assess the effectiveness of ENA-based design and metrics for integrated building energy systems. This process is represented by the iteration loop from *Redesign* to *Engineering system* in Figure 3. Redesign decisions are motivated from the network analysis and high-level ENA metrics. For some examples, we look for opportunities to increase link density and resource sharing, reduce exergy destruction and exergy flows, and improve waste-heat capture. These decisions are visible in either

Table 1: Traditional and ENA-based KPI evaluated in this research.

	Indicator	Units	Eq.
Traditional	Power usage effectiveness (PUE)	–	(16)
	Site/source energy efficiency ($\eta_{I,sit}$, $\eta_{I,sou}$)	%	(18)
	Source exergy efficiency ($\eta_{II,sou}$)	%	(2)
	Source energy use (E_{sou})	Wh	(20)
	Unmet hours (t_{unm})	h	(21)
ENA	Capacity (c)	nats	(7)
	Ascendancy (a)	nats	(8)
	Reserve (ϕ)	nats	(9)
	Total system throughput (Ψ)	Wh	(10)
	Degree of system order (α)	%	(13)
	Finn's Cycling Index (FCI)	%	(14)

the network graphs or the ENA metrics, such as increasing the Finn's Cycling Index (presented in section 3). After selecting a new system design, we then revisit each stage in Figure 3, updating model equations as needed, validating the new design, and reassessing performance.

3. Mathematical Formulation

This section presents the ENA formulation that was developed in Step 2 (section 2.2) for building and community energy systems. While buildings are the intended domain of the authors, this formulation is suitable for any complex dynamic engineering system. More specifically, the mathematics in sections 3.1– 3.3 are written generically for any conserved system involving mass and/or energy. If the system involves heterogeneous flows, care must be taken to aggregate units on an *apples-to-apples* basis. As such, section 3.4 presents an exergy-based formulation for aggregating multiple energy types of various (and time-varying) qualities.

3.1. Nomenclature

With biomimetics, it is common that the mathematical languages used in the biological sciences differ from those used in the technical applications. Thus, care must be taken to select a common language. As much as possible, we aimed to follow standard mathematical notation for the targeted technical audience, while maintaining variable assignments from ENA's biological origins. Following similar variable assignments as those adopted by [12] and [7], we define n as the number of functional compartments at time t, with compartment index $i \in 1, ..., n$; $x(t, \cdot)$ as the total storage in compartment i at time t; $\dot{f}_{ij}(t, \cdot)$ as the *non-negative* flow rate from compartment i to j at time t; $\dot{y}_i(t, \cdot) = \dot{f}_{i0}(t, \cdot)$ as the flow rate leaving the system boundary ($j = 0$) from compartment i at time t; $\dot{z}_i(t, \cdot) = \dot{f}_{0i}(t, \cdot)$ as the flow rate entering the system boundary ($j = 0$) from compartment i at time t; and $\dot{d}_i(t, \cdot) = \dot{f}_{i,n+1}(t, \cdot)$ as the dissipation (i.e., losses) flow rate ($j = n + 1$) from compartment i at time t. Figure 4 visualizes this nomenclature in a theoretical network.

In addition to the above variable assignments, several standard nomenclature from the targeted engineering audience are adopted. Following thermodynamics standards, lower case letters indicate an intensive, unit-basis property (e.g., x is exergy stored per unit mass [J/kg]), while upper case

letters indicate an extensive, mass-basis property (e.g., X is total exergy stored [J]). Following thermofluid sciences, a dot above the variable indicates a flow rate (e.g., $\dot{f}$ corresponds to power [W], while f corresponds to energy [J]). Thus, over simulation period $t \in [t_1, t_2)$, it follows that

$$f_{ij} = \int_{t_1}^{t_2} \dot{f}_{ij}(t, \cdot) dt. \tag{1}$$

For multivariate functions, a center dot as in $f_i(\cdot)$ is used to indicate that f is dependent on several other independent variables, which tends to vary across all i compartments.

3.2. Network Structure and Flows

Figure 4 depicts our suggested system boundary for ENA in a building's context, with flows to and from two compartments. We define the system boundary such that the exergy efficiency on a source basis $\eta_{II,sou}$ is

$$\eta_{II,sou} = \frac{\sum f_{0i}}{\sum f_{i0}} = \frac{\text{(end use outputs)+(useful exports)}}{\text{(primary energy inputs)}}. \tag{2}$$

Examples of end use exports, useful exports (to other heterogeneous systems), and primary energy inputs are given in Figure 4. In this work, we adopt the definition for *primary energy* by Standard 105 [50], which is

> *site energy plus the estimated energy consumed or lost in extraction, processing, and transportation of primary energy forms such as coal, oil, natural gas, biomass, and nuclear fuel; energy consumed in conversion to electricity; and energy consumed or lost in transmission and distribution to the building site.*

This definition is also equivalent to the U.S. Department of Energy's *full-fuel-cycle* and is consistent with *source energy* for zero energy buildings [51]. The resolution of compartment boundaries can be selected based on the modeler's needs and data availability. For example, a district energy simulation may lump the HVAC system for each building as one compartment, while a single building simulation may represent each equipment as one compartment.

For any compartment i, the governing system of equations for is

$$\frac{dX_i}{dt} = \underbrace{\left(\dot{z}_i(t, \cdot) + \sum_{j=1}^{n} \dot{f}_{ji}(t, \cdot) \right)}_{\text{inward flow rates}} - \underbrace{\left(\dot{y}_i(t, \cdot) + \dot{d}_i(t, \cdot) + \sum_{j=1}^{n} \dot{f}_{ij}(t, \cdot) \right)}_{\text{outward flow rates}} \tag{3}$$

$$X_i(t_0) = X_{i,0}, \; \forall \, i = 1, ..., n, \tag{4}$$

where X_i is the useful energy (i.e., exergy) stored in compartment i at time t; the first summation represents all inward flow rates to i; the second summation represents all outward flow rates from i; and Eq. (4) encompasses the initial conditions. Here, subscript 0 represent the initial state. By convention, any flow $\dot{f}_{ij}(t, \cdot) \geq 0$. Further explanation on the need for exergy analysis is given in section 3.4.

The above relationships are defined at a compartment level. For system-level analysis, we also define the following matrices. For compartmental storages, $\mathbf{X} = [X_1(t, \cdot), ..., X_n(t, \cdot)]^{\mathrm{T}}$ represents

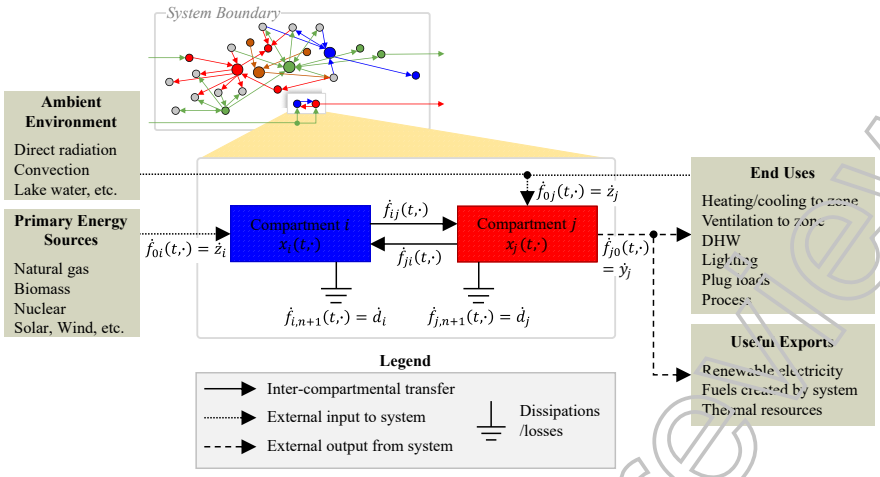

Figure 4: Demonstration network graph with flow definitions with respect to two of the 26 compartments. This includes external inputs, external outputs, inter-compartmental transfers, and dissipations. The system boundary is defined in a building's context.

the state vector with initial conditions $\mathbf{X}(t_0) = \mathbf{X_0} = [X_{1,0}, ..., X_{n,0}]^{\mathrm{T}}$. Here, 0 represents the initial state and T indicates the matrix transpose. Similarly, the output, input, and dissipation flow rate vectors are $\dot{\mathbf{y}} = [\dot{y}_1(t,\cdot), ..., \dot{y}_n(t,\cdot)]^{\mathrm{T}}$, $\dot{\mathbf{z}} = [\dot{z}_1(t,\cdot), ..., \dot{z}_n(t,\cdot)]^{\mathrm{T}}$, and $\dot{\mathbf{d}} = [\dot{d}_1(t,\cdot), ..., \dot{d}_n(t,\cdot)]^{\mathrm{T}}$, respectively. Representing the set of all internal flows between compartments, the *direct flow matrix* $\mathbf{F_r}$ of size $n \times n$ is $\mathbf{F_r} = (f_{ij})$ with $1 \leq i, j \leq n$. Encompassing all flows, the *total flow matrix* is $\mathbf{F} = (f_{ij})$ with $0 \leq i, j \leq n+1$. Including variable assignments y_i, z_i, and d_i, $\mathbf{F}$ expands as

$$\mathbf{F} = \begin{array}{c} \begin{matrix} 0 & 1 & 2 & \cdots & \cdots & n{+}1 \end{matrix} \\ \begin{bmatrix} 0 & z_1 & \cdots & \cdots & z_n & 0 \\ y_1 & 0 & f_{12} & \cdots & f_{1n} & d_1 \\ \vdots & f_{21} & \ddots & \vdots & f_{2n} & \vdots \\ \vdots & \vdots & \vdots & \vdots & \vdots & \vdots \\ y_n & f_{n1} & \cdots & f_{n-1,n} & 0 & d_n \\ 0 & 0 & \cdots & \cdots & 0 & 0 \end{bmatrix} \end{array}. \tag{5}$$

For this system, the differential algebraic system of equations is

$$\frac{d\mathbf{X}}{dt} = \dot{\mathbf{F}}_{\mathbf{r}}^{\mathrm{T}}\mathbf{1} + \dot{\mathbf{z}} - \left(\dot{\mathbf{F}}_{\mathbf{r}}\mathbf{1} + \dot{\mathbf{y}} + \dot{\mathbf{d}}\right), \tag{6}$$

where $\mathbf{1}$ represents a column vector of length n with all elements equal to 1.

3.3. Ecological Network Analysis

Beyond structure and flows, ENA leverages information theory to quantify the organization of conserved properties in complex networks. In standard ENA, the foundational metrics are the

capacity for system development c, the *ascendancy* a, and the *overhead* ϕ. Defined in [7], these are

$$c = -\sum_{i=0}^{n+1}\sum_{j=0}^{n+1} \frac{f_{ij}}{\Psi} \ln\left(\frac{f_{ij}}{\Psi}\right), \tag{7}$$

$$a = \sum_{i=0}^{n+1}\sum_{j=0}^{n+1} \frac{f_{ij}}{\Psi} \ln\left(\frac{\Psi f_{ij}}{\tau_{out,i}\tau_{in,j}}\right), \text{ and} \tag{8}$$

$$\phi = -\sum_{i=0}^{n+1}\sum_{j=0}^{n+1} \frac{f_{ij}}{\Psi} \ln\left(\frac{f_{ij}^2}{\tau_{out,i}\tau_{in,j}}\right), \tag{9}$$

where the *total system throughput* Ψ is

$$\Psi = \sum_{i=0}^{n+1}\sum_{j=0}^{n+1} f_{ij}, \tag{10}$$

and the total *inward* and *outward throughflows* at compartment i are

$$\tau_{in,i} = \sum_{j=0}^{n+1} f_{ji} \quad \text{and} \tag{11}$$

$$\tau_{out,i} = \sum_{j=0}^{n+1} f_{ij}. \tag{12}$$

Here, we adopt the comprehensive definition by others [7, 52, 53], where Ψ represents the sum of all fluxes occurring in the system over the designated time period $t \in [t_1, t_2)$, including system inputs/outputs and dissipations.

One of the most useful metrics in ENA is the *degree of system order*, given as

$$\alpha = \frac{a}{c}. \tag{13}$$

In words, α is a unitless ratio that represents the *organization* (or the lack of flow diversity) in a networked system. By definition, the decomposition of capacity is $c = a + \phi$. Thus, it is guaranteed that $\alpha \in [0, 1]$ because $a \leq c$ and $c, a, \phi \geq 0$. Degree of system order has been adopted in several works as an effective metric to compare order across different systems [14] and for evaluating resiliency [34]. With this basis, previous ENA literature identified a *window of vitality* for biological ecosystems that clustered in $25\% \lesssim \alpha \lesssim 53\%$ [11]. Previous ENA studies show that ecosystems falling in this range are at an optimal balance between redundancy (low α) and efficiency (high α), and that this range can be considered a desirable level of organization for sustainable growth and development [54].

Lastly, Finn's Cycling Index FCI "accounts for the percentage of all [flows] that is generated by cycling" [53]. Mathematically, FCI is

$$FCI = \sum_{i=1}^{n} \frac{\tau_{in,i}}{\Psi}\left(\frac{l_{ii} - 1}{l_{ii}}\right), \tag{14}$$

where l_{ii} is the ith entry along the diagonal of the Leontief matrix $\mathbf{L} = [\mathbf{I} - \mathbf{G}]^{-1}$, with identity matrix $\mathbf{I}$ and *fractional inflow matrix* $\mathbf{G} = (f_{ij}/\tau_{in,i})$. For 100 ecosystem models, [15] found that FCI ranged from 0–98% with a mean of 38%. While this finding does not provide static target, [18] suggests that FCI increases with stress for natural ecosystems. For engineering systems, this leads to a hypothesis that FCI may be a useful operational objective during stressful events, but testing this hypothesis is out of the scope of this paper.

Equations (7)-(14) are standard ENA. In our work, we replace steady state f_{ij} with dynamically-calculated, multivariate functions using Eq. (1), which is novel for engineering applications of ENA. This extends [12], where network structure and flows were defined dynamically, but ENA metrics were excluded. In addition, we advance [12] from ecological systems with low-order ordinary differential equations to engineering systems with stiff, hybrid differential algebraic equations. Furthermore, because the translation from information theory to ENA is at times obscure, we graphically depict several ENA metrics as a Venn diagram in Figure 5. In the information theory context, a is equivalent to *mutual information*, c is equivalent to *joint entropy*, and ϕ is equivalent to *conditional entropy*. In short, mutual information is the information obtained in the flow origin (destination) by knowing the destination (origin); joint entropy is the expected uncertainty in all possible flow paths; and conditional entropy is the uncertainty that remains when we either know the flow origin or destination. Further, α can be visually interpreted from Figure 5 as the ratio of $\mathbb{I} \cap \mathbb{J}$ to $\mathbb{I} \cup \mathbb{J}$; in the information theory context, α is equivalent to the *Jaccard Index*. Interested readers can find more on information theory in [55].

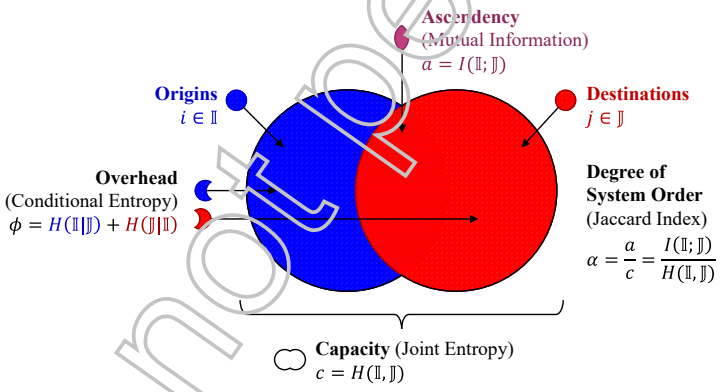

Figure 5: Venn diagram showing relationships of ENA (and corresponding information theory) metrics.

In addition, there are a few notable differences between this and previous ENA works. First, we adopt Ψ for total system throughput instead of the commonly-used T, because T is used for temperature in thermofluid sciences. Second, extrinsic ENA metrics are often used (C, A, and Φ), where $A = a\Psi$ encompasses both the "total activity" through Ψ and the "organization by which component processes are linked" through a [18]. Instead, we adopt the intrinsic versions (c, a, and ϕ) to maintain equivalence with information theory and allow the results to be extensible to other system types and sizes, similar to [56]. Third, ENA metrics allow for several logarithmic bases to be appropriate. While $\log_2(\cdot)$ is often selected – such as in [7], where the units for a, c, and ϕ are *bits* – we keep consistency with data science and engineering practices by adopting $\ln(\cdot)$ (base e with units of *nats*).

3.4. Exergy-Based Approach for Integrated Thermofluid–Electrical Systems

In sections 3.1 through 3.3, the mathematical formulations are applicable for any conserved quantity (i.e., materials, energy, carbon, currency, etc.). While previous adoptions of ENA performed the analysis on an energy basis, ENA applications involving *multiple dynamic energy types* is the most meaningful if the analysis is on an *exergy* basis. For reference, *energy* is the extensive, conserved quantity that is inter-convertible with heat and work, and *exergy* is the potential of an energy resource to do work with respect to the surroundings. As such, exergy captures not only the *quantity* of energy but also the *quality*. For ENA of dynamic energy systems with multiple energy qualities (e.g., electricity and thermofluids), exergy analysis is critical for two main reasons. First, a given quantum of electrical energy can do more work than the same quantum of thermofluid energy; when integrating these two energy types in the same framework, energy-based analysis will over estimate the value of heat and fluid resources, while exergy analysis fairly reflects the quality. Second, the useful work of heat and fluid resources change significantly over time due to temperature and humidity fluctuations in the ambient environment and engineering systems. This is particularly true for building systems, where temperature states are in close proximity to the ambient environment. As such, fixed conversion factors such as TCE can grossly over or under estimate an energy resource's value, while exergy correctly captures changes in quality over time.

While exergy has not yet been used as a basis for ENA, it is worth noting that exergy analysis outside of ENA is well established. [57] provides a comprehensive reference on exergy analysis across a diverse range of engineering and biological applications, including power generation, transportation, land biomass, the human body, and more. For a building's context, interested readers can find more information in [58]. Among the diversity of exergy applications, there naturally are discrepancies on methodologies and assumptions. Our approach for this work is as follows. First, we assume the dead state is the current outdoor air temperature rather than a fixed temperature. This provides the most meaningful formulation because (1) exergy is concerned with the portion of energy that has the potential to do work with respect to the surroundings, and (2) operating temperatures for building systems are frequently near ambient conditions. As such, it is worth noting that exergy of the system can increase by the system moving further from the dead state, or the dead state moving further from the system. Second, we assume exergy is always positive. This ensures that all $f_{ij} \geq 0$, consistent with ENA standards and the standard conceptualization that all useful work is positive.

This work adopts a generic balance for the exergy X in compartment i as

$$\frac{dX_i}{dt} = \sum_k \left(1 - \frac{T_0}{T_k}\right)\dot{Q}_k \tag{15a}$$

$$- \left(\dot{W} - p_0 \frac{dV_{cv}}{dt}\right) \tag{15b}$$

$$+ \sum_j \dot{m}_j \left|(h_j - h_0) - T_0\,(s_j - s_0)\right| \tag{15c}$$

$$- \dot{X}_f \tag{15d}$$

$$+ \dot{X}_{ke} + \dot{X}_{pe} \tag{15e}$$

$$- \dot{X}_d, \tag{15f}$$

where the right hand terms in Eq. (15) represent the heat transfer (15a), the useful and boundary

work (15b), the thermofluid inflow and outflow (15c), the chemical exergy of fuels (15d), the kinetic and potential energy (15e), and the exergy destruction (15f). Temperature is T, pressure is p, volume is V, heat flow rate is $\dot{Q}$, work rate is $\dot{W}$, mass flow rate is $\dot{m}$, specific enthlapy is h, and specific entropy is s. For subscripts, 0 is the dead state, cv is the control volume, ke is kinetic energy, pe is potential energy, and d is destruction. In Eq. (15c), we formulate the thermofluid exergy with absolute values to maintain all $f_{ij} \geq 0$ whether the fluid is cold or hot relative to the dead state [59].

It is worth noting that Eq. (3) and Eq. (15) represent different forms of the same balance equation. While Eq. (3) represents a generic control volume balance for any conserved property (e.g., mass, energy), Eq. (15) represents the exergy control volume balance. In essence, the left-hand terms dX_i/dt are identical, while the right-hand terms in (15a)-(15f) are the available exergy flows that can be present in any right-hand term of Eq. (3). As an example, section 7 of the Appendix shows how each flow equation involves one or more components of Eq. (15).

4. Case Study

We demonstrate the new ENA capabilities for the design of heating and cooling systems for an office building and data center located in Denver, Colorado, USA. Denver represents a semi-arid climate (Köppen climate classification of *BSk*) with a historical average 2350 kWh/m^2 of direct solar radiation each year. The following sections present the physical and control systems as well as the Modelica implementations. Building upon open source models from the Modelica Buildings Library (MBL) [45] v9.0.0 and Modelica Standard Library (MSL) v4.0.0, we constructed system and ENA models in Modelica. Path references to the open-source models are provided below when available.

As the initial baseline case, the data center and office building have separate HVAC systems, representing efficient yet common configurations present today. Following the methodology in Figure 3, we progressively redesign the heating and cooling systems based on ENA insights (i.e., increase network connectivity, conserve exergy flows, etc.). This process resulted in three redesign cases, all which use an ambient-loop DES to share energy resources. After understanding the case study systems, each system is then mapped to a network digraph in section 4.5.

4.1. Baseline Model: Separate Systems

4.1.1. Physical System

The baseline system involves a standalone data center and an office building. Depicted in Figure 6a, the baseline data center 500kW server room that is cooled with a primary-only chiller plant. This data center cooling system is open-source in the MBL as *IntegratedPrimaryLoadSideEconomizer* within the *Applications/DataCenters* package. The chiller plant contains two parallel chillers, an integrated water-side economizer (WSE) on the load side, two parallel cooling towers, two parallel condenser water (CW) pumps, two parallel chilled water (CHW) pumps, and an air handling unit (AHU). The AHU – also known as a computer room air handler (CRAH) – contains a cooling coil, humidifier, a variable-speed fan, and an electric re-heater. For the computer room, only the heat exchange between the cooling system and servers are modeled because the heat transfer between the room and the ambient environment is negligible compared to heat released by the servers.

Depicted in Figure 6b, the baseline office model has a single-zone variable air volume (VAV) HVAC system with air-side economizing, hydronic cooling, and electric heating. The office HVAC

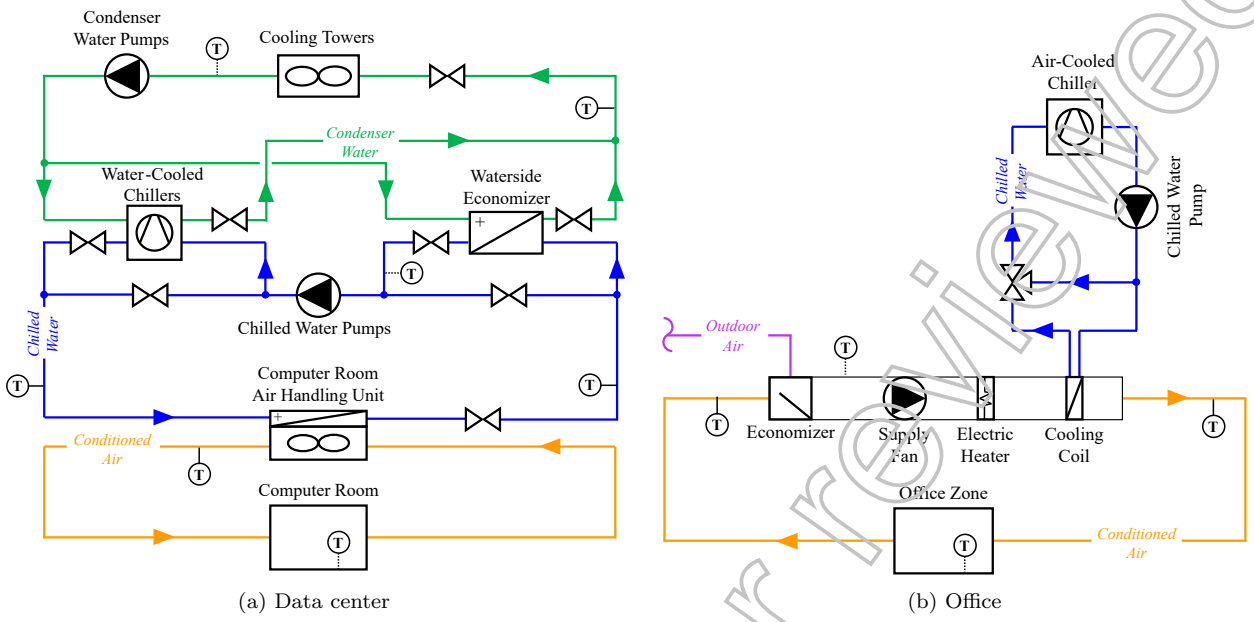

(a) Data center (b) Office

Figure 6: Schematics of the data center and office building.

system model is available in the MBL as *ChillerDXHeatingEconomizer* within the *Air* package. The office thermal zone model was generated automatically with TEASER [60] and represents a variation of *SimpleRoomTwoElements* within the *ThermalZones/ReducedOrder* package of the MBL. More specifically, the reduced order RC thermal zone is modeled as a simple room defined in Guideline VDI 6007 Part 1 [61] with two heat conduction elements (exterior walls, interior walls). Zone air temperature T_{ZA} is determined based on the transient thermal conditions due to the envelope, HVAC system, and internal loads (people and electrical equipment). Solar radiation on tilted surfaces are calculated from the TMY3 weather file.

All components used in the data center and office systems are publicly available in the MBL. While complete information regarding component model equations, design principles, and assumptions are available in the MBL documentation, some of the major equipment models are described here. For both the office building and data center, the electric chillers – named *ElectricEIR* in the MBL – are based on the DOE-2.1 chiller model with three polynomial functions to determine capacity and power consumption [62]. Both buildings also implement ideal mass flow controlled pumps – MBL model *FlowControlled_m_flow* – where the mass flow is input directly, and power performance is calculated from user-specified performance curves and robust affinity law formulations [63]. In the data center, cooling towers are modeled based on the variable speed Merkel model in EnergyPlus version 8.9.0 [64], which determines the total heat transfer between air and water entering the tower based on Merkel's theory. Lastly, the office air-side economizer and chilled water three-way valve are modeled as ideal valves with a prescribed valve position based on the ratio of mass flow through the bypass leg.

4.1.2. Controls

For the data center chiller plant, the master-level control (Figure 7) determines the cooling mode of the entire plant. When the plant is on, it is operating in one of three states: free cooling (only WSE), partial-mechanical cooling (WSE and chillers), or mechanical cooling (only

chillers). As shown in Figure 7, the logic for switching states is based on the condition of the chilled water supply and return temperatures to the WSE (T_{CHWS} and T_{CHWR}, respectively) with a waiting time of 20 minutes. Switching conditions include the chilled water supply temperature setpoint $T_{CHWS,set}$, the measured T_{CHWS}, the measured ambient wetbulb temperature T_{WB}, and the approach temperature T_{app} For this plant, $T_{CHWS,set}$ and T_{app} are 8°C and 6°C, respectively.

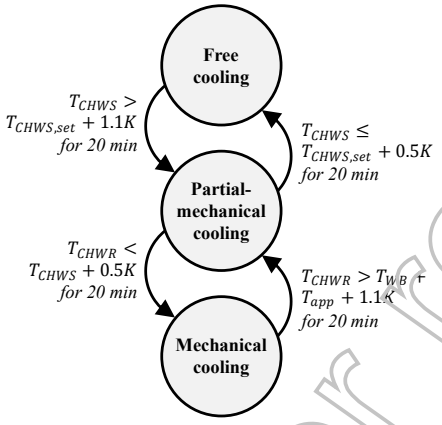

Figure 7: Master-level control to determine the cooling mode for the data center chiller plant.

Following from the master-level cooling mode control, the chiller plant cooling system also contains staging and unit level controls. The principal logics are as follows. In partial-mechanical or mechanical cooling modes, at least one chiller is on, and two chillers are on if the load is larger than 55% of the nominal; one of the chillers switch off if the load drops below 30% of the nominal. For the constant-speed CW pumps, the number of pumps running equals the number of chillers running. For the variable-speed CHW pumps, pumps are staged based on the speed signal and mass flow rate. The CHW mass flow rate is modulated with a PI controller to maintain a differential pressure at the AHU of 80 kPa. Lastly, the AHU fan speed is modulated with a PI controller to maintain the room temperature at 25°C.

For the baseline office HVAC system, the controls involve various speed and temperature controls as well as economizing control. The control model is *ControllerChillerDXHeatingEconomizer* in *Air/Systems/SingleZone/VAV/BaseClasses* package of the MBL. Schedules determine the supply air temperature setpoint $T_{SA,set}$ during heating/cooling modes with setback temperatures during unoccupied hours. The cooling control valve and electric heater are modulated with separate PI controllers to maintain $T_{SA,set}$ during cooling and heating modes, respectively. During cooling, the chiller maintains the CHW supply temperature at a fixed setpoint of 6°C. During heating, the AHU fan is always on, while it is controlled with PI during cooling to maintain the zone air temperature setpoint (measured at the return). Lastly, the economizer maintains the minimum outdoor air fraction of 40%, unless the system is in cooling mode and the outdoor air is cooler than both the mixed and return air temperatures. In the later case, the economizer controls maintain the mixed temperature at $T_{SA,set} = 13$°C by increasing the outdoor air fraction up to 100%.

4.2. Redesign Model 1: DES Constant Flow

4.2.1. Physical System

The first redesign integrates an ambient DES with a geothermal borefield for storage. The heating/cooling system schematics for the top-level DES, data center, and office are shown in Figure 8. At the district level, the office, data center, and geothermal borefield are connected to an

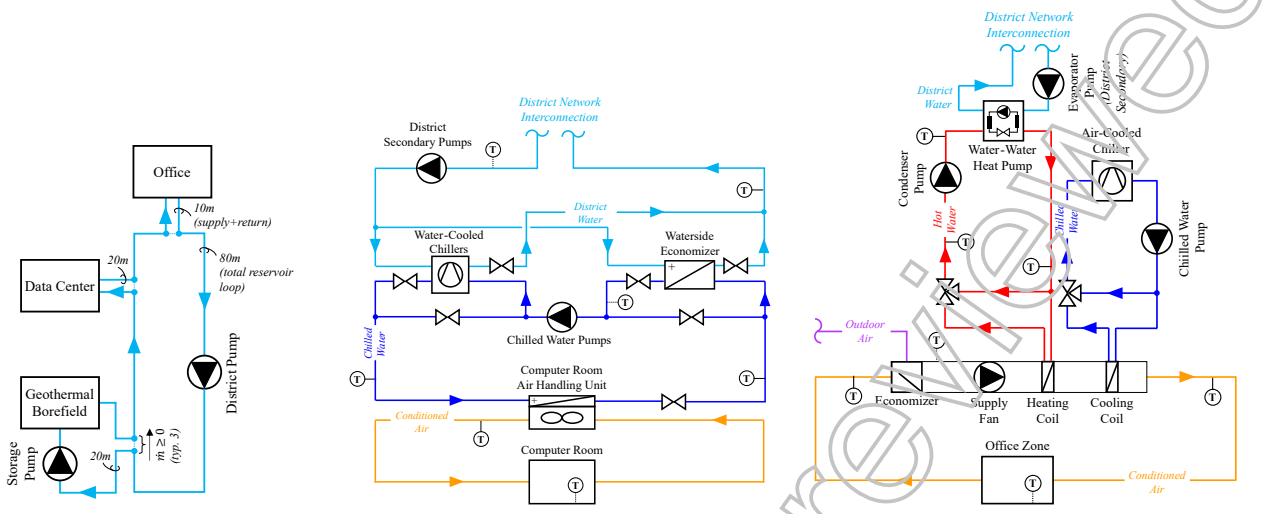

(a) District (b) Data Center (c) Office

Figure 8: Schematic diagrams for Redesign 1 and 2.

ambient-loop DES with unidirectional flow. This DES system, specifically titled a *reservoir network* in [65], allows a floating network temperature from 6-17°C. From an implementation standpoint, the reservoir network is favorable because it avoids the unstable pressure coupling between district and building fluid systems that can arise in bidirectional DES [66]. The DES piping network was constructed with custom instances of *Buildings.Experimental.DHC.Networks.Combined.BaseClasses.ConnectionSeriesStandard*, where the standard pipes were replaced with plug flow pipes using the model *Buildings.Fluid.FixedResistances.PlugFlowPipe*. Developed with DHC in mind, this pipe model efficiently and accurately evaluates pipe pressure drop, heat transfer through the pipe walls, and fluid transport delay. More information on the plug flow modeling approach and assumptions can be found in [67].

The data center, office, and borefield physical systems are as follows. As shown in Figure 8b, the data center model is similar to the baseline, except that the cooling towers are replaced with a direct DES interconnection. Similarly, the office building also represents a variation on the baseline model, except that the electric heating coil is replaced with a hydronic coil (Figure 8c). For office heating, a water-to-water heat pump with a bypass loop are used to supply hot water to the hydronic coil and maintain the supply air temperature. Lastly, the geothermal borefield provides storage capabilities and stabilizes the district network temperature. Oriented vertically, the borefield contains 350 vertical boreholes with heights of 300 m and diameters of 190 mm. This borefield is an instance of *Buildings.Experimental.DHC.Plants.Reservoir.BoreField*; further information regarding the borefield configuration and assumptions are available in the MBL documentation.

While all of the case study systems are implemented hierarchically in Modelica, we provide Figure 9 as an example for a top-level, runnable model. This model diagram contains the complete system and ENA compartments in orange (both on the left). Post-processing blocks are on the right, where the ENA compartments are mapped to matrices representing the inter-compartmental transfers, inputs, outputs, and dissipations. All downstream ENA metrics are calculated from the matrix representation using the relationships described in section 3.

Furthermore, Figure 10 shows examples of lower-level models. Figure 10a is the internal diagram

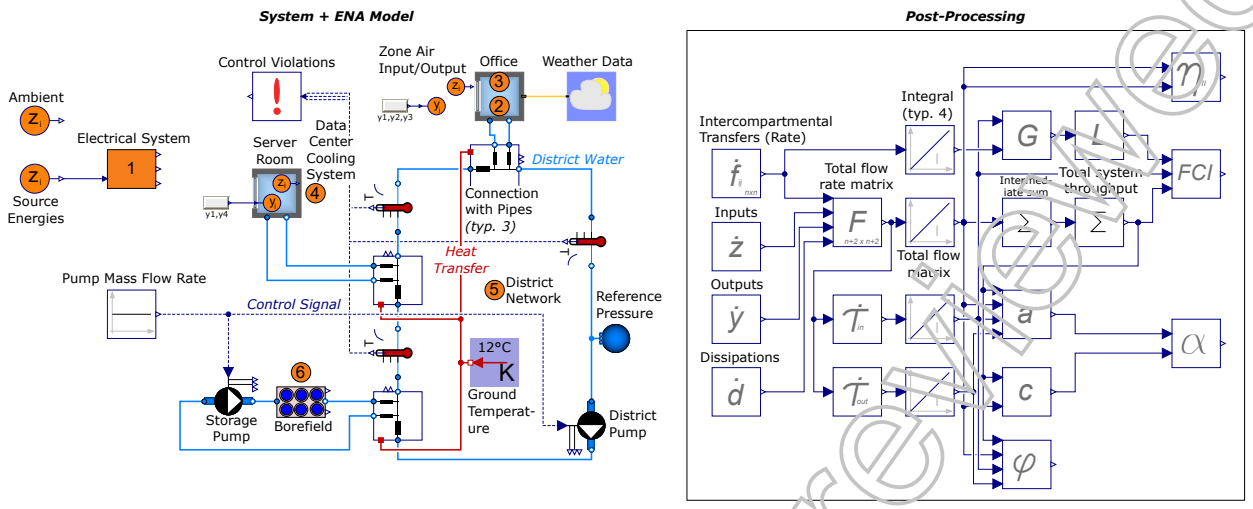

Figure 9: Modelica diagram of the system model for Redesign 1 with ENA compartment blocks in orange. Post-processing blocks common to every simulation model are on the right.

of the *Office* block from Figure 9; while Figure 10b is the internal diagram of the *HVAC* block from Figure 10a. Together, these diagrams represent three levels of the hierarchical model. These models were constructed with components of the MBL. Namely, the heat pump implements *Carnot_TCon* which prescribes the condenser leaving temperature. The performance is determined based on the Carnot efficiency and a polynomial-based efficiency-factor for part load conditions.

4.2.2. Controls

Controls for the DES, borefield, data center, and office building were adjusted according to the system redesign. In the district network loop and borefield, the pumps maintain a constant flow rate such that the flow across the bypass at any interconnection is greater or equal to zero (indicated with the dashed lines in Figure 8a). For the data center, the existing hierarchical controls from the baseline case were retained without modifications.

For the office building, the chiller and cooling control valve controls are the same as the baseline case, but the heating and economizer controls are modified. The heat pump is controlled with PI to maintain temperature differences of 5°C on both the evaporator and condenser sides. As depicted in Figure 10a, the heating system also contains hot water reset controls such that the hot water supply temperature ramps up from 28°C to 38°C proportional to heating load changes from 0% to 100% of nominal. Lastly, similar to the cooling three-way valve, the heating valve is modulated with a PI controller to maintain the zone air temperature at the heating setpoint.

4.3. Redesign Model 2: DES Variable Flow

This case has the same system, network structure, and network flows as *Redesign Model 1* (section 4.2), except for the controls for the DES main circulation pump and borefield pump. Instead of the constant speed pumps in Redesign 1, this pump control reduces the pump speed unless the water temperature measurements are either too high or too low. Shown in Figure 11, this pump controller reduces the speed unless the mix temperatures are either too high or too low, in which case the pump speed is increased to the maximum. In addition, the control implements a temperature shift to increase the total efficiency if there is net heating or cooling on the loop. This

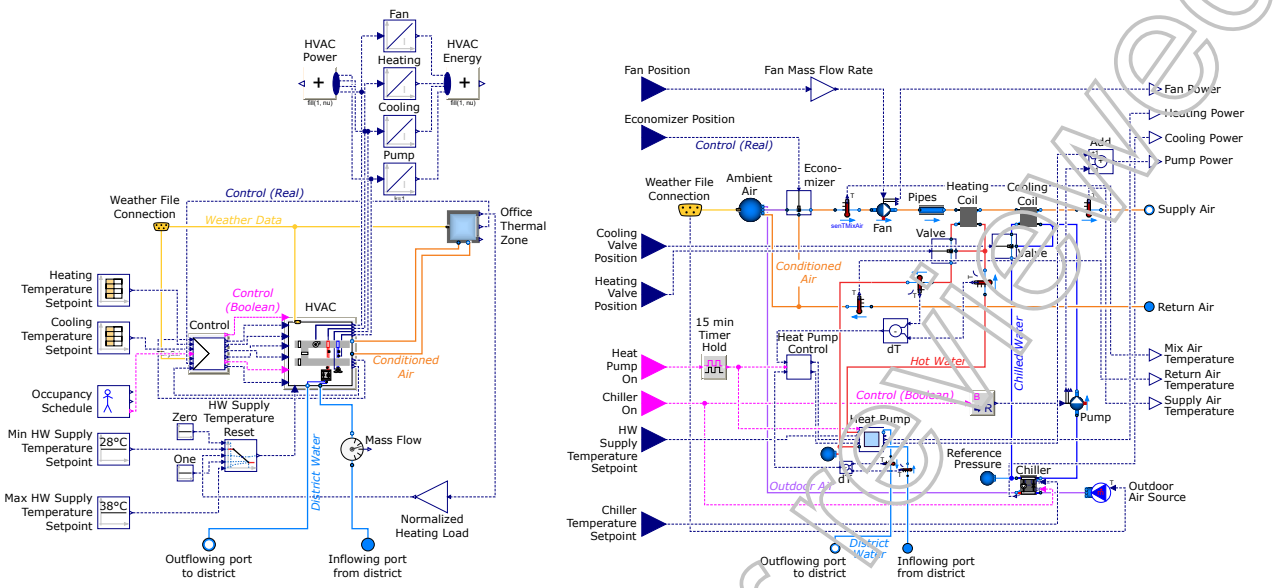

(a) Office Zone and HVAC (b) Office HVAC

Figure 10: Modelica diagrams of the office building and HVAC subsystem.

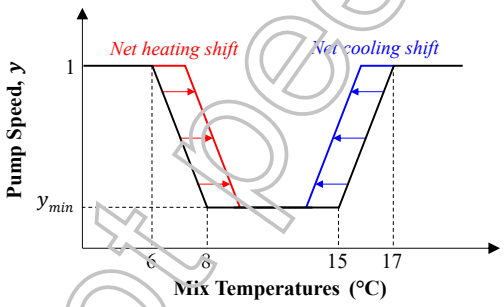

Figure 11: Control logic for Redesign 2 with variable speed pump control at the district and geothermal borefield.

control follows the logic of *Buildings.Experimental.DHC.Networks.Controls.MainPump*, except that instead of a fixed minimum speed, we implement a variable minimum speed y_{min} such that the mass flow through the district loop is never lower than the minimum mass flow for any connection. This ensure that primary overflow is ensured at every district connection.

4.4. Redesign Model 3: Liquid Cooling

This case is the same as *Redesign Model 1* (section 4.2), except the data center cooling system is changed from air to liquid cooling with a direct connection, as shown in Figure 12. Liquid cooling covers a wide-variety of technologies for data center cooling systems. As the name implies, liquid cooling systems involve liquid mediums (typically water or water-glycol mixtures) that exchange heat with the server racks directly. In this case study, we model a system similar to the dual-enclosure-liquid cooling system [68] with all computer devices cooled with liquid; except, the DES system is used to reject the heat rather than cooling towers. The district secondary and server pumps are modulated with a single PI controller to maintain liquid environment through the server

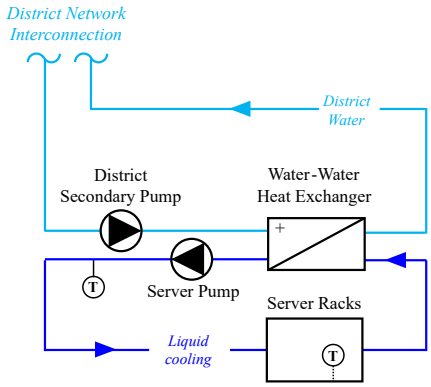

Figure 12: Schematic diagram for the data center liquid cooling system in redesign 3.

racks at 25°C, the same temperature as the previous three cases. The heat exchanger assumes a constant effectiveness of 80%.

4.5. Network Structure and Flows

For each design, we developed digraphs representing the network structures (Figure 13). Colors are used to distinguish major systems, while line types indicate the type of flow. The baseline model has one structure (Figure 13a), and all three redesign cases can be represented by the same network structure (Figure 13b). In these systems, all compartments have dissipations (indicated with electrical ground symbols), but dynamics are not negligible for only some of the compartments (indicated with ascetics). For example, the office envelope has high thermal mass that greatly influences the amplitude and time delays of exergy transfer with the office zone air. In contrast, the exergy storage in the AHU is small compared to other compartments and can be neglected.

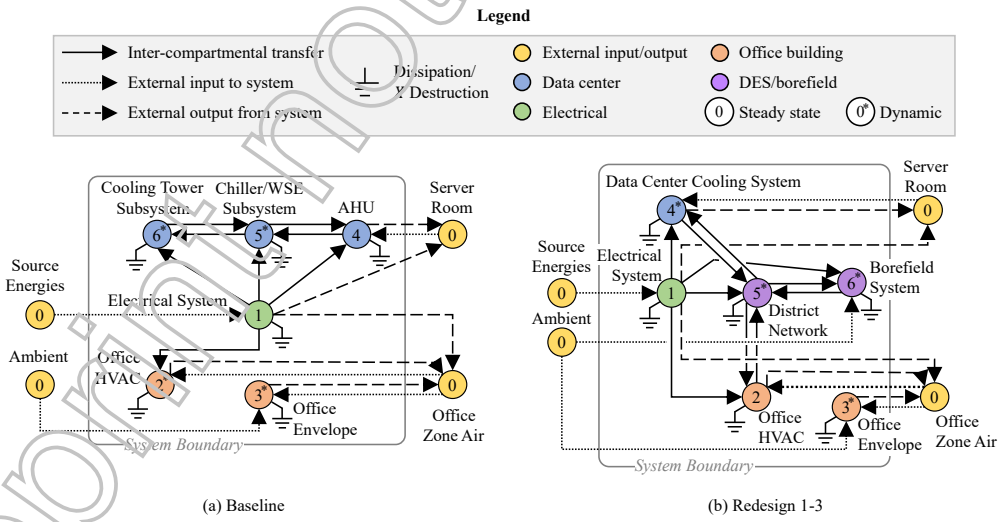

Figure 13: Network digraphs for all four case studies. All three redesign cases can be represented by the structure shown in (b); only the edge weights, flow types (air vs. water), and storages will differ. The data center cooling system is dynamic in redesign 1-2 but steady state in redesign 3.

The flows for all edges in Figure 13 are defined using the relevant exergy balance components

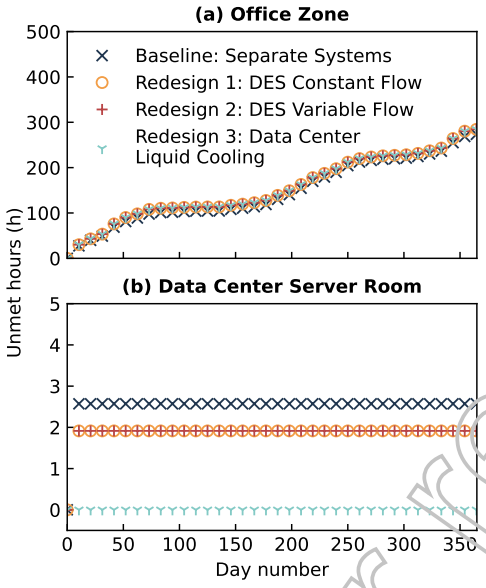

Figure 14: Unmet hours in the office and data center for the four systems.

from Eq. (15) and the nomenclature defined in Figure 4. All network equations for the four case studies are included in Table 5 and Table 6 of the Appendix. At a high level, we provide equations for all inter-compartmental transfers, external inputs, external outputs, and storages. Based on the compartmental exergy-balance and network graph, the solver calculates dissipations for all compartments at each time step. Lastly, section 3.4 presents all assumptions for the exergy-based ENA implementation.

5. Results

5.1. System Performance

In addition to providing power for equipment, the primary function of these systems is to meet HVAC needs. More specifically, the redesign provides alternative methods for heating, cooling, and resource sharing by improving network structure and flows. As shown in Figure 14, the accumulative unmet hours for all systems and both buildings stayed below the 300 hour limit per Standard 90.1 [49]. For the office building, the three redesign cases produced only 11 more unmet hours relative to the baseline case. For the data center, all systems maintained the constant setpoint throughout the year, staying below 5 unmet hours.

With sample weeks from both winter and summer seasons, Figure 15 shows further details on how each system design was able to meet the thermal performance. For the office zone, the temperature setpoint changes both daily and seasonally; all systems effectively adjusted to the setpoint (Figure 15a). For the data center server room (Figure 15b), all systems maintained the 25°C setpoint. In the geothermal borefield (Figure 15c), the mean annual temperature for all redesign systems was 13.5-13.6°C with an annual range of 1.7-1.8°C. As expected, the average borefield temperature was lower in the winter than the summer. Lastly, the district piping network (Figure 15d) remained within the desired range of 6-17°C throughout the year.

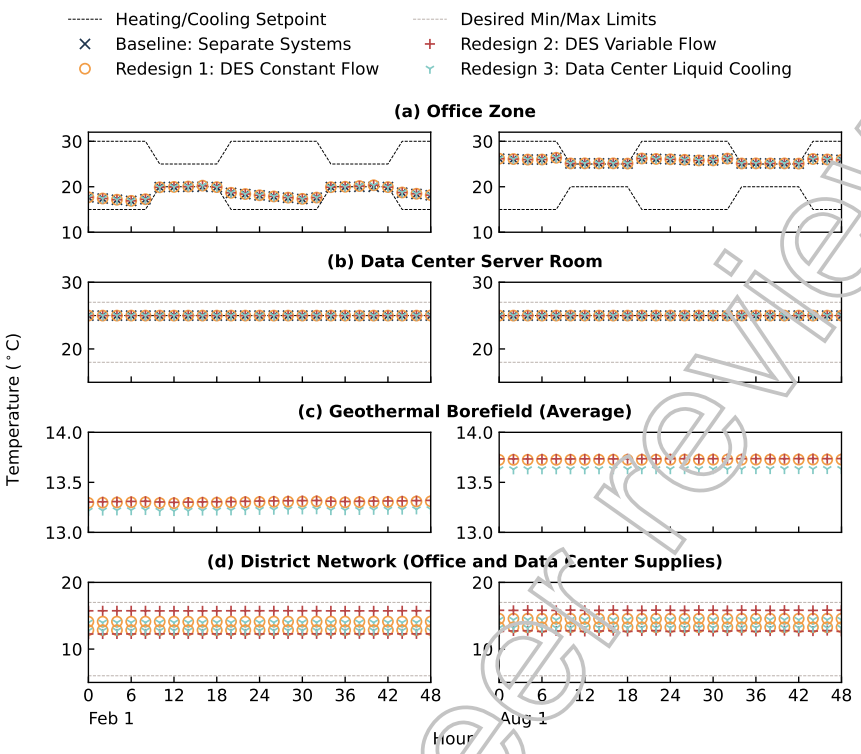

Figure 15: Temperature results from typical winter (left) and summer (right) days.

In addition to thermal performance, the systems were also evaluated in terms of traditional efficiency-based metrics and HVAC energy consumption. Table 2 summarizes the several efficiency-based metrics for the data center and entire system. With PUE values under 1.2, all included data center systems are considered efficient [69]. Redesign 3 with liquid cooling achieved the lowest PUE at 1.01; while 1.01 is theoretically possible, the lowest PUE of real-world data centers known to the authors is 1.02 [70]. Energy efficiency increased modestly on both site and source bases from baseline to redesign 3. Unexpectedly, exergy efficiency decreased significantly from baseline (60.29%) to redesign 3 (34.34%). This decrease in exergy efficiency occurred because the decrease in exergy delivered to the server room – numerator of Eq. (2) – was relatively greater than the decrease in exergy supplied to the site – denominator of Eq. (2). In contrast, the numerator of Eq. (18) is held constant for both site and source energy efficiency metrics (i.e., the energy demand does not change), while only the denominator decreases (i.e., the energy input required to meet the demand is reduced).

Furthermore, Figure 16 breaks downs the HVAC energy on a monthly basis. For the baseline case (Figure 16a), the data center cooling towers consumed the most energy (32%), followed by the chillers (25%). Over the year, the data center was in mechanical cooling, free cooling, and partial mechanical cooling mode for 1.0%, 31%, and 68% of the year, respectively. Heating accounted for 64% of the site energy of the office building in the baseline case. For redesign cases 1 and 2 (Figures 16a-b) without changes to the control logic, the data center operated in partial mechanical cooling for 100% of the year. In these cases, the data center pumps were the dominate consumer (44-46%) due to the increased hours with the high-pressure pathway through chillers and WSE; the

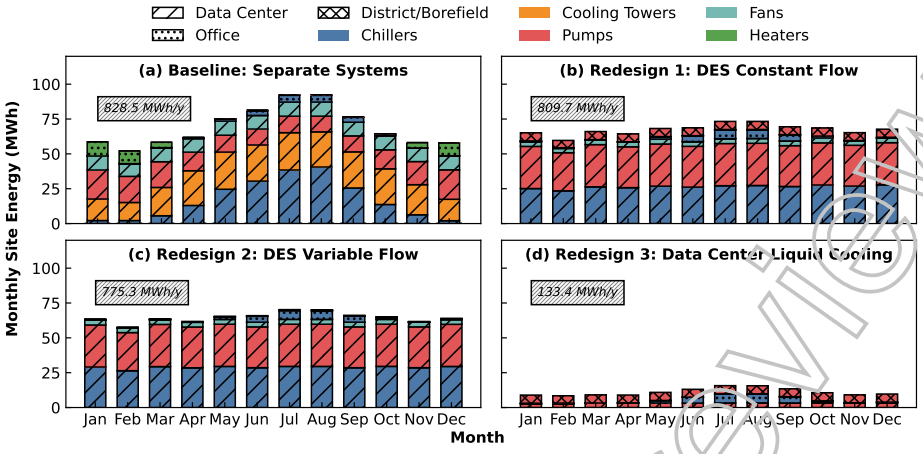

Figure 16: Monthly site energy consumption for HVAC equipment across the four case studies. Hatch patterns indicate the equipment location. Color indicates the equipment type. Annual HVAC site energy totals are indicated in the gray boxes.

Table 2: Traditional efficiency-based results for system performance. Equations for these traditional metrics are include in the Appendix.

Case	PUE	$\eta_{I,sit}$ (%)	$\eta_{I,sou}$ (%)	$\eta_{II,sou}$ (%)
Baseline	1.18	85.48	31.20	60.29
Redesign 1	1.16	85.79	31.31	50.66
Redesign 2	1.17	86.36	31.52	51.15
Redesign 3	1.01	98.56	35.97	34.34

chillers were the next highest consumer at 39-45%. Relative to the other cases, the HVAC system for redesign 3 consumed drastically less energy (133.4 MWh/y, 84% less than the baseline). This is largely due to the elimination of several equipment in the data center cooling system, including the chillers, WSE, AHU, cooling towers, fans, and CW pumps. Despite a large pressure drop in the data center liquid cooling racks, the pumping energy also reduced notably compared to the air cooled systems. In Figures 16a-c, the data center pumping energy is dominated by the CW pumps, while these pumps are eliminated in Figure 16d. More specifically, the liquid cooling takes advantage of low mass flow (average $\dot{m}_{DWS} = 10.1$ kg/s) and high temperature change ($\Delta T_{DWS} = 11.75$°C); meanwhile the air cooled systems have high CW mass flow ($\dot{m}_{CWS} = 70.0$ kg/s) and low CW temperature change ($\Delta T_{CWS} = 1.82$°C).

5.2. Network Structure and Flows

Figure 17 shows the annual exergy flows for each case study system as weighted directed graphs. To aid interpretation, all edges with flows less than 5% of the maximum flow is shown in gray for each system. Across all systems, the largest exergy flow was from source energies to the electrical system (f_{01}). The exergy destruction at the electrical system was also significant for all systems (f_{17}). Interestingly, the simple cycle with supply air (SA) (f_{40}) and return air (RA) (f_{40}) flows from the AHU to the server room in Figures 13a-c were high-exergy flows. This result motivated the change from air to liquid cooling at the data center with redesign 3.

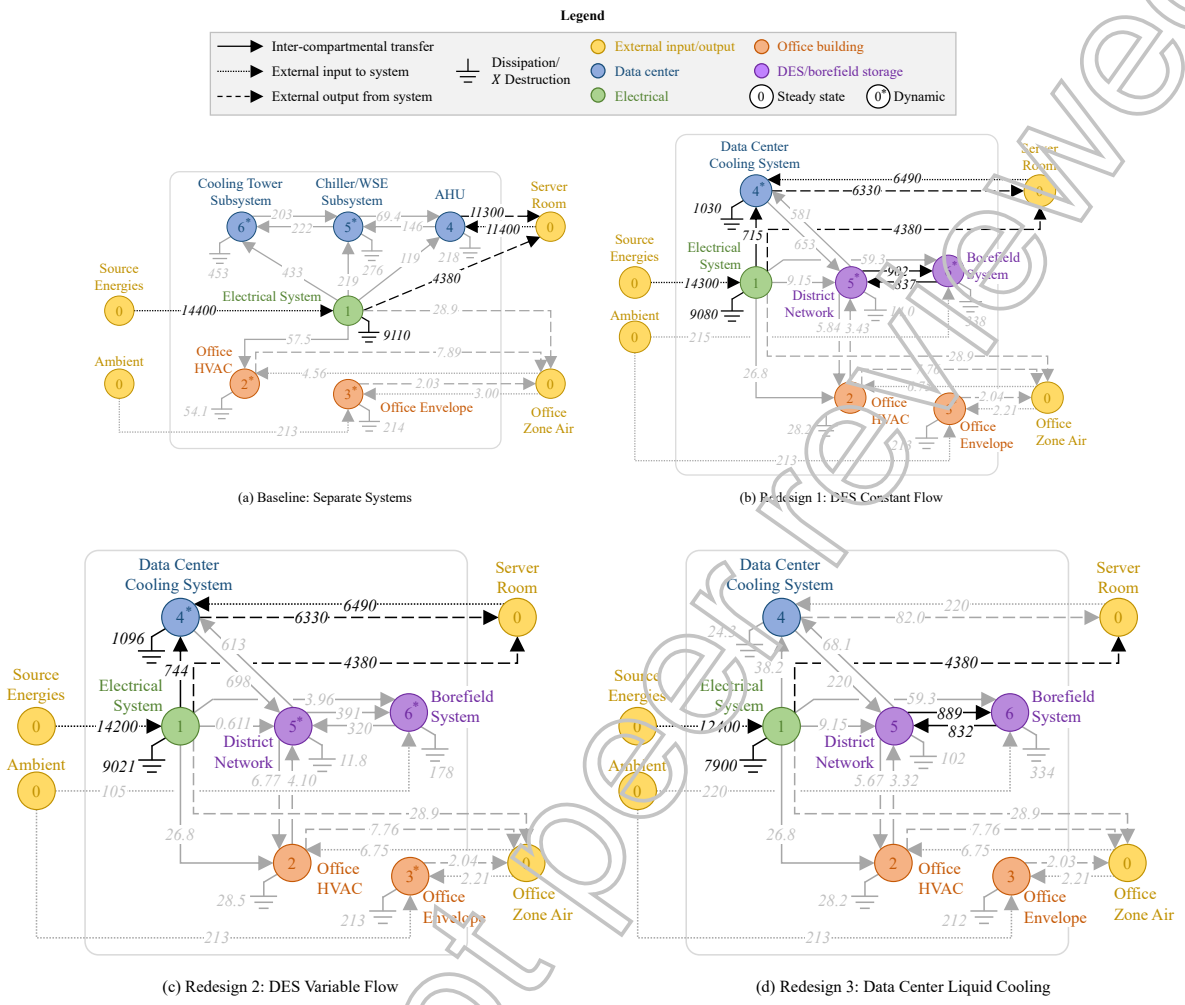

Figure 17: Network digraphs of annual exergy (MWh) for the four systems. Flows $f_{ij} < 0.05 \max(f_{ij})$ are in gray.

Two findings are important to understand why the data center SA and RA were high exergy. First, we note that the *exergy difference* between supply and return air streams is small ($f_{04} - f_{40} =$ 163 MWh) relative to each stream (e.g., $f_{40} =$ 11300 MWh). Redesign 3 with liquid cooling produces a comparable result ($f_{04} - f_{40} =$ 153 MWh in Figure 13d). This follows expectations because the cooling system needs to remove the same heat from the data center servers across all cases, while the small differences are due to variations in pumping energy. Second, the conditioned air loop is high exergy compared to the water loops in Figures 17a and d due to two interrelated factors:

1. the mass fraction of water in the conditioned air is *3.4 times* higher than the average outdoor air mass fraction due to humidification in the AHU and
2. $T_{RA} > T_{SA} > T_{CHWS}$ and often $T_{RA}, T_{SA} \gg T_0$.

In contrast, the exergy flows f_{04} and f_{40} in Figure 17d are significantly reduced by changing the data center cooling from air to liquid water.

Several prominent flows from Figure 17 are selected for further dynamic analyses, presented in Figure 18. Across all systems, the input from source energies to the electrical system remained relatively constant due to the dominance of the data center server equipment load. In contrast, the RA from the server room ($\dot{f}_{04}$) and the SA to the server room ($\dot{f}_{40}$) – present in Figures 17a-c – exhibited larger daily and seasonal fluctuations. Further, because of the small exergy difference between the RA and SA, these flows are indistinguishable in Figure 17. In the systems with constant pumping at the DES and borefield (Figures 17b and d), the supply water to the borefield ($\dot{f}_{56}$) and return water from the borefield ($\dot{f}_{65}$) presented large fluctuations in exergy flow.

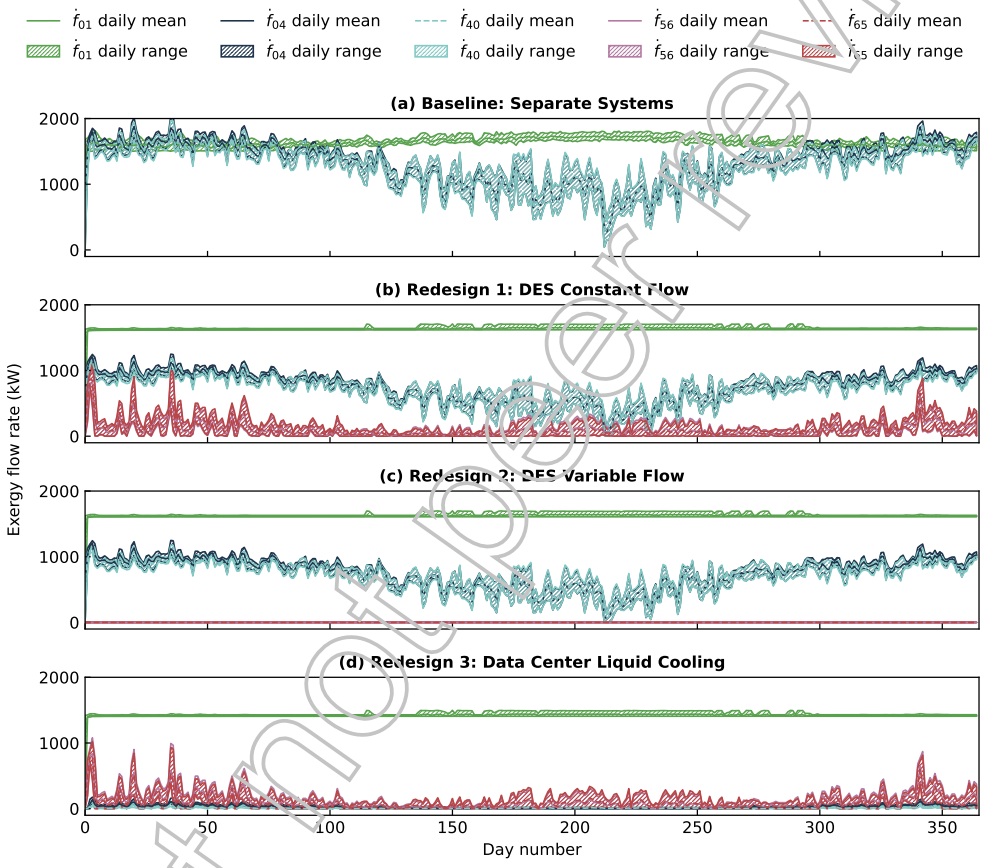

Figure 18: Daily means and ranges of exergy flow rates of dominant edges from Figure 17.

5.3. ENA Metrics

Table 3 summarizes the ENA metrics for all case study systems. From baseline to redesign 3, Ψ progressively decreased, indicating the redesign process successfully reduced the total exergy consumed in the network. Because redesign 1 and 2 produced the highest c values, these systems had the highest degree of uncertainty among all possible flow paths. At the same time, a also increased in redesign 1 and 2 compared to the baseline; as a result, $\alpha = a/c$ decreased by 2% from the baseline to redesign 1 and 2. Of all the systems, redesign 3 had the lowest c, while a remained fairly constant; as such redesign 3 and the highest α at 56.1%, indicating that this system is *more efficient* than the others in terms of *network organization*.

Table 3: ENA metrics over annual simulations with the baseline and three redesign cases.

Metric	Base	Re. 1	Re. 2	Re. 3	Units
Ψ	53500	46700	45300	28400	MWh/y
c	1.81	2.04	1.97	1.56	nats
a	0.849	0.916	0.875	0.876	nats
ϕ	0.964	1.13	1.10	0.685	nats
α	46.8	44.9	44.4	56.1	%
FCI	0.317	5.07	3.63	5.08	%

Interconnecting the office and data center HVAC systems via DES allowed new opportunities for cycling in the network. In Table 3, FCI for the baseline was 0.317%. When DES was added to the system with constant flow pumps (redesign 1 and 3), FCI increased to 5.07-5.08%. When the DES and borefield pumping was changed from constant speed (redesign 1) to variable speed (redesign 2), the DES network and borefield moved less thermofluid through the system. This in turn caused FCI to decrease to 3.63%. Despite the fact that electrical load for the data center servers dominates all flow paths, the addition of DES with a geothermal borefield for storage enabled significant increases in FCI, which may have resiliency benefits during disruptive events [18].

6. Discussion

Through a biomimetic approach, this work systematically adapted and translated ENA from biological sciences for dynamic engineering system applications. By this process, we found that both ENA and the graph theoretic methods at its foundation add new analysis perspectives for designing building and community energy systems. To bridge the research gap, two principle scientific innovations were required. First, we formulated ENA for dynamic engineering systems and demonstrated a Modelica-based implementation with a complex system model that is typical in real-world engineering practice. To the authors' knowledge, only [36] has applied ENA dynamically for a technical application to date; this work provides a second successful case, while also demonstrating the application of ENA with a new software tool with greater capabilities for solving large, complex, multi-physical system models. Second, we implemented ENA on an exergy basis to aggregate heterogeneous energy types with often time-varying qualities. From our literature review (Table 4), aggregation methods to date consisted of weighted sums, unweighted sums, and products. These static methods cannot capture temporal changes in nor the rich diversity of many energy types, including thermofluids, heat transfer, and boundary work. For ENA of building energy systems, exergy analysis is the physically correct representation to capture important energy quality differences and dynamics. This work demonstrated the value of exergy analysis to ENA for the first time.

While exergy analysis enhanced ENA in this work, it is also possible that ENA can enhance exergy analysis. Traditionally, exergy analysis stems from heat engines and combustion cycles [57]. In these cases, two physical features largely determine the analysis approach: (1) the operating temperature of the heat reservoir is far from the ambient; and (2) as a network graph, simple cycles represent most systems. Due to these factors, exergy analysis predominantly assumes a constant dead state and reduces the problem to a series of $A \rightarrow B$ processes. The calculated exergy destruction (i.e., entropy generated) is then due to each process. Several modern *LowEx* [71] engineering systems – and biological systems by nature – operate near ambient conditions, which brings the

assumed dead state temperature into question. This work reinforces that the variable ambient air temperature is most appropriate for near-ambient systems, as previously recommended by [71]. Further, ENA encompasses entire networked systems, where the capacity (i.e., joint entropy) represents the average level of *uncertainty* across the network's set of origins and destinations (as shown in Figure 5). Extending the deterministic *process-based* approach of exergy analysis today, ENA contributes probability *network-based* uncertainty, with compatible origins from the second law of thermodynamics as described in [7].

From this case study with thermofluid-electrical systems in the built environment, the findings show that ENA can provide valuable insights. With the developed approach, we designed the heating and cooling systems for a data center and office building case study, coupling the building systems together via an ambient-loop DES with a geothermal borefield for storage. The results indicated that ambient-loop DES can greatly increase network cycling (FCI from 0.317% to 5.08%). Further, the degree of system order α progressively increased through the redesign process from 46.8% to 56.1%, indicating that this site benefited from higher network efficiency. Though this ENA-inspired redesign process, the total system throughput Ψ decreased by 47.0% from 53500 MWh/y to 28400 MWh/y. The site HVAC energy also decreased by 84% from 829 MWh/y to 133 MWh/y. Quantification of network organization through FCI and α informed design decisions, as well as exergy observations in the network graphs of Figure 17. This case study showcases the value of ENA to aid engineers in making informed whole-system decisions for integrated energy systems.

Surprisingly, this case study revealed problems for using traditional efficiency-based metrics when designing complex, low-exergy systems. While all efficiency metrics represent a ratio of outputs to inputs, what quantities constitute those outputs/inputs depends on the system. For example, PUE is common for data centers, heat engines adopt a ratio of work out to heat in, and heat pumps use a coefficient of performance (heat out over work in), while air conditioning systems typically use a (seasonal) energy efficiency ratio (power input over cooling capacity output). When many of these systems are combined on one site, selecting the correct inputs/outputs can at times be unclear. To address this challenge, many consider exergy efficiency to be a more universal metric with applicability for multiple energy systems because it is *model independent* [72]. However, for this case study, exergy efficiency *decreased* from 60.3% to 34.3% with system improvement. This is counter intuitive but understandable from a system's perspective. While maintaining equivalent performance (same thermal comfort), redesign 3 with liquid cooling required less exergy output than the baseline case with separate systems. Because the exergy output decreased in higher proportion than the exergy input, exergy efficiency also decreased. For building and community energy systems – particularly low-exergy systems – these results indicate critical shortcomings of traditional efficiency-based metrics.

There are important limitations of this study to consider. The purpose of this study was to evaluate ENA for building and community energy systems rather than innovating HVAC system designs. Because of this, further evaluations are necessary before adopting redesign cases 1-3. Regarding redesign cases 1-2, the cooling towers from the baseline were replaced with DES interconnections; however, no changes were made to adjust controls, which caused the systems to operate in partial-mechanical cooling mode for the entire year. Before these system configurations could be implementable in real-world practice, further control redesign would be required at a minimum. Regarding the liquid cooling case (redesign 3), despite the significant improvement that this case showed compared to data center air cooling, detailed design and further system validation

is required before any firm conclusions can be drawn. This system assumed all server equipment can be cooled with liquid directly; while this is theoretically possible, some existing equipment require internal fans by design. With that said, the HVAC energy savings achieved by switching to liquid cooling are on par with DELC systems; for example, [68] developed and experimentally evaluated a DELC technology which demonstrated over 90% energy savings compared to conventional refrigeration-based technologies. This work reinforces their findings from a whole-systems perspective, and indicates that ambient-loop DES could provide new opportunities to capture low-quality waste heat from data centers that would otherwise be lost to environment (i.e., through cooling towers).

Extending this work, future research is merited to understand ENA comprehensively across engineering sciences, evaluate new use cases for dynamic ENA, and ideate future whole-system models for building and community energy systems. This paper demonstrated three system redesigns for district-scale heating and cooling systems. First and foremost, additional case studies are needed to evaluate ENA across the diversity of energy and building systems (i.e., climates, density, functions, system designs). For example, previous empirically-evaluated ecosystem models identified a *window of vitality* from $25\% \lesssim \alpha \lesssim 53\%$ [11]; three of the four systems in this paper fell within this range, except for redesign 3, which fell just outside the upper bound at $\alpha = 56.1\%$. However, the diversity of *complex systems* in this world is high, and for biological systems,"it has yet to be investigated whether any sub-regions of the window might be preferred over others" [14, p. 32]. As such the critical question remaining is not *does my system fall within the window of vitality*; but instead, *how does the window of vitality change for different system types, geographies, and stress conditions*. The later question has yet to be evaluated, to our knowledge. Second, several use cases for the design and operation of building energy systems may use ENA in the future. In a design context, future studies may leverage network information to select technology investments (e.g., add PV or storage, recycle waste energy) or classify building types for connected communities. For operational purposes, it would be interesting to evaluate the benefits of α and FCI for determining system response strategies under stress. Lastly, this work translated ENA for engineering system applications, but we did not innovate new mathematics beyond the existing ENA scope. There are opportunities to improve ENA in the future by, for example, revising the information theoretic dimensionality from two to higher-order set – as also suggested by [18] – or mapping system development to panarchy models and adaptive cycles – as done in a non-ENA biological context by [73]. With the transition of energy and building systems towards dynamic, interconnected, zero-emission systems, innovative methods such as ENA has the potential to support several design and operational scenarios in the future.

7. Conclusion

This work is the first to adopt ENA for building applications, and one of the first to apply dynamic ENA for engineering applications. Network graph methods like ENA can provide the building simulation community new complex system information (e.g., degree of cycling, network organization, etc.) that has benefits beyond the efficiency-based metrics that dominate today. We advance ENA research by implementing an exergy-based approach for heterogeneous energy systems, formulating ENA dynamically for engineering applications in comprehensive mathematical models, and implementing those models with Modelica, which is suitable for large, stiff systems of equations. For a case study, we demonstrate our ENA implementation by iteratively designing the heating and cooling systems for an office building and data center. The simulation results indicate

that the four system designs have equivalent thermal performance, while 84% of HVAC site energy can be saved by connecting the buildings together via ambient-loop district energy and changing the data center from air to liquid cooling. Surprisingly, exergy efficiency decreased through the system improvement, because the decrease in exergy delivered to the server room (output) was relatively greater than the decrease in exergy supplied to the site (input) for the redesign cases. This indicates traditional input/output metrics may miss important information for high-performance, low-exergy building and community energy systems. By ENA metrics, the final system design increased cycling in the network and operated at a higher degree of system order. For future studies, we conclude that this ENA approach is highly scalable from the equipment-level to national grids. While network analysis is promising for building and community energy systems, further research is needed to understand the suitability of high-level ENA metrics across the diversity of building applications (e.g., different climates, building functions, critical/non-critical loads). For zero-carbon and resilient building systems of the future, ENA can provide new insights for network organization, which may outperform traditional efficiency-based metrics.

Acknowledgment

This research was supported in part by an appointment with the IBUILD Graduate Student Research Program sponsored by the U.S. Department of Energy (DOE), Office of Energy Efficiency and Renewable Energy, and Building Technologies Office. This program is managed by Oak Ridge National Laboratory (ORNL). This program is administered by the Oak Ridge Institute for Science and Education (ORISE) for the DOE. ORISE is managed by ORAU under DOE contract number DESC0014664. All opinions expressed in this paper are the author's and do not necessarily reflect the policies and views of DOE, ORNL, ORAU, or ORISE. This material is also based upon work supported by the National Science Foundation under Award No. 2025459. Lastly, this work emerged from the IBPSA Project 1, an international project conducted under the umbrella of the International Building Performance Simulation Association (IBPSA). Project 1 will develop and demonstrate a BIM/GIS and Modelica Framework for building and community energy system design and operation.

References

[1] M. Wetter, A View on Future Building System Modeling and Simulation, in: J. L. M. Hensen, R. Lamberts (Eds.), Building Performance Simulation for Design and Operation, Taylor & Francis Group, Routledge, UK, 2011, Ch. 17.

[2] IEA, World Energy Outlook 2019, Tech. rep., IEA, Paris (2019).
URL https://www.iea.org/reports/world-energy-outlook-2019

[3] S. O. Muhanji, A. Muzhikyan, A. M. Farid, Distributed Control for Distributed Energy Resources: Long-Term Challenges and Lessons Learned, IEEE Access 6 (2018) 32737–32753. doi:10.1109/ACCESS.2018.2843720.

[4] Y. Fu, S. Huang, D. Vrabie, W. Zuo, Coupling Power System Dynamics and Building Dynamics to Enabling Building to Grid Integration, in: The 13th International Modelica Conference, Regensburg, Germany, 2019, pp. 561–566. doi:10.3384/ecp19157561.

[5] K. M. Tan, V. K. Ramachandaramurthy, J. Y. Yong, Integration of electric vehicles in smart grid: A review on vehicle to grid technologies and optimization techniques, Renewable and Sustainable Energy Reviews 53 (2016) 720–732. doi:10.1016/j.rser.2015.09.012.

[6] F. Dalyan, I. Macgill, R. Amal, Opportunities and Challenges for Renewable Power-to-X, ACS Energy Letters 5 (12) (2020) 3843–3847. doi:10.1021/acsenergylett.0c02249.

[7] R. E. Ulanowicz, Growth and Development: Ecosystems Phenomenology, Springer-Verlag, New York, 1986. doi:10.1007/978-1-4612-4916-0.

[8] S. R. Borrett, L. Sheble, J. Moody, E. C. Anway, Bibliometric review of ecological network analysis: 2010–2016, Ecological Modelling 382 (2018) 63–82. doi:10.1016/j.ecolmodel.2018.04.020.

[9] A. Layton, B. Bras, M. Weissburg, Designing Industrial Networks Using Ecological Food Web Metrics, Environmental Science and Technology 50 (20) (2016) 11243–11252. doi:10.1021/acs.est.6b03066.

[10] A. Chatterjee, A. Layton, Mimicking nature for resilient resource and infrastructure network design, Reliability Engineering and System Safety 204 (2020) 107142. doi:10.1016/j.ress.2020.107142.

[11] A. Chatterjee, H. Huang, K. R. Davis, A. Layton, A Multigraph Modeling Approach to Enable Ecological Network Analysis of Cyber Physical Power Networks, in: IEEE International Conference on Communications, Control, and Computing Technologies for Smart Grids (SmartGridComm), 2021, pp. 239–244. doi:10.1109/SmartGridComm51999.2021.9631989.

[12] H. Coskun, Dynamic ecological system analysis: A holistic analysis of compartmental systems, Heliyon 5 (9) (2019) e02347. doi:10.1016/j.heliyon.2019.e02347.

[13] B. D. Fath, U. M. Scharler, R. E. Ulanowicz, B. Hannon, Ecological network analysis: network construction, Ecological Modelling 208 (1) (2007) 49–55. doi:10.1016/j.ecolmodel.2007.04.029.

[14] R. E. Ulanowicz, S. J. Goerner, B. Lietaer, R. Gomez, Quantifying sustainability: Resilience, efficiency and the return of information theory, Ecological Complexity 6 (1) (2009) 27–36. doi:10.1016/j.ecocom.2008.10.005.

[15] S. R. Borrett, M. K. Lau, enaR: An R package for Ecosystem Network Analysis, Methods in Ecology and Evolution 5 (11) (2014) 1206–1213. doi:10.1111/2041-210X.12282.

[16] V. Christensen, D. Pauly, ECOPATH II - a software for balancing steady-state ecosystem models and calculating network characteristics, Ecological Modelling 61 (1992) 169–185. doi:10.1016/0304-3800(92)90016-8.

[17] B. D. Fath, S. R. Borrett, A MATLAB function for Network Environ Analysis, Environmental Modelling and Software 21 (2006) 375–405. doi:10.1016/j.envsoft.2004.11.007.

[18] R. E. Ulanowicz, Quantitative methods for ecological network analysis, Computational Biology and Chemistry 28 (2004) 321–339. doi:10.1016/j.compbiolchem.2004.09.001.

[19] L. Matamba, C. Kazanci, J. R. Schramski, M. Blessing, P. Alexander, B. C. Patten, Throughflow analysis: A stochastic approach, Ecological Modelling 220 (22) (2009) 3174–3181. doi:10.1016/j.ecolmodel.2009.07.001.

[20] C. Kazanci, Q. Ma, Extending ecological network analysis measures to dynamic ecosystem models, Ecological Modelling 242 (2012) 180–188. doi:10.1016/j.ecolmodel.2012.05.021.

[21] T. G. Hallam, M. N. Antonios, An environ analysis for nonlinear compartment models, Bulletin of Mathematical Biology 47 (6) (1985) 739–748. doi:10.1007/BF02469300.

[22] H. Coskun, Nonlinear decomposition principle and fundamental matrix solutions for dynamic compartmental systems, Discrete and Continuous Dynamical Systems - Series B 24 (12) (2019) 6553–6605. doi:10.3934/dcdsb.2019155.

[23] isee systems, Stella and iThink Version 3.3 with Assemblies and Completion Support (2022).
URL https://iseesystems.com/resources/help/v3/Default.htm

[24] W. Yang, S. Wang, B. Chen, Embodied carbon emission analysis of eco-industrial park based on input-output analysis and ecological network analysis, in: The 9th International Conference on Applied Energy, ICAE2017, Vol. 142, Cardiff, UK, 2017, pp. 3102–3107. doi:10.1016/j.egypro.2017.12.451.

[25] L. Liang, Y. Xu, B. Liu, C. Liu, M. Luther, Y. Xu, Embodied energy-based ecological network analysis on growth and development of the national industrial system: An empirical study in Australia, Journal of Cleaner Production 324 (2021) 129253. doi:10.1016/j.jclepro.2021.129253.

[26] Y. Zhang, Z. Yang, B. D. Fath, Ecological network analysis of an urban water metabolic system: Model development, and a case study for Beijing, Science of the Total Environment 408 (2010) 4702–4711. doi:10.1016/j.scitotenv.2010.06.019.

[27] X. Zhu, X. Mu, G. Hu, Ecological network analysis of urban energy metabolic system—A case study of Beijing, Ecological Modelling 404 (100) (2019) 36–45. doi:10.1016/j.ecolmodel.2019.04.016.

[28] S. Wang, Y. Liu, B. Chen, Multiregional input–output and ecological network analyses for regional energy–water nexus within China, Applied Energy 227 (19) (2018) 353–364. doi:10.1016/j.apenergy.2017.11.093.

[29] X. Yu, Y. Liu, Z. Zhang, Y. Xiong, M. Dang, Urban spatial structure features in Qinling mountain area based on ecological network analysis-case study of Shangluo City, Alexandria Engineering Journal 61 (12) (2022) 12829–12845. doi:10.1016/j.aej.2022.06.049.

[30] S. Wang, B. Chen, Energy–water nexus of urban agglomeration based on multiregional input–output tables and ecological network analysis: A case study of the Beijing–Tianjin–Hebei region, Applied Energy 178 (2016) 773–783. doi:10.1016/j.apenergy.2016.06.112.

[31] S. Chen, B. Chen, Urban energy consumption: Different insights from energy flow analysis, input-output analysis and ecological network analysis, Applied Energy 138 (2015) 99–107. doi:10.1016/j.apenergy.2014.10.055.

[32] A. Li, H. Zheng, Energy security and sustainable design of urban systems based on ecological network analysis, Ecological Indicators 129 (2021) 107903. doi:10.1016/j.ecolind.2021.107903.
[33] G. Hyde, B. D. Fath, Ecological Network Analysis of State-Level Energy Consumption in Maryland, USA, Energies 15 (2022) 5995. doi:10.3390/en15165995.
[34] A. Chatterjee, R. Malak, A. Layton, Ecology-inspired resilient and affordable system of systems using degree of system order, Systems Engineering 25 (1) (2022) 3–18. doi:10.1002/sys.21598.
[35] T. Dave, A. Layton, Bio-inspired design for resilient water distribution networks, in: The 26th CIRP Life Cycle Engineering (LCE) Conference, Vol. 80, 2019, pp. 275–280. doi:10.1016/j.procir.2019.01.020.
[36] B. C. Watson, S. Malone, M. Weissburg, B. Bras, Adding a Detrital Actor to Increase System of System Resilience: A Case Study Test of a Biologically Inspired Design Heuristic to Guide Sociotechnical Network Evolution, Journal of Mechanical Design 142 (December) (2020) 121705. doi:10.1115/1.4048579.
[37] H. Huang, V. Panyam, M. R. Narimani, A. Layton, K. R. Davis, Mixed-Integer Optimization for Bio-Inspired Robust Power Network Design, in: 2020 52nd North American Power Symposium (NAPS), 2021, pp. 1–6. doi:10.1109/NAPS50074.2021.9449755.
[38] V. Panyam, H. Huang, K. Davis, A. Layton, Bio-inspired design for robust power grid networks, Applied Energy 251 (2019) 113349. doi:10.1016/j.apenergy.2019.113349.
[39] The AnyLogic Company, AnyLogic Documentation (2023).
URL https://anylogic.help/
[40] S. E. Mattsson, H. Elmqvist, Modelica – An international effort to design the next generation modeling language, in: 7th IFAC Symposium on Computer Aided Control Systems Design (CACSD '97), Vol. 30, Gent, Belgium, 1997, pp. 151–155. doi:10.1016/S1474-6670(17)43628-7.
[41] ISO/TC 266, Biomimetics — Terminology, concepts and methodology, 1st Edition, Vol. 18458, ISO, 2015.
[42] F. E. Cellier, E. Kofman, Continuous System Simulation, Springer, New York, NY, USA, 2006.
[43] J. W. Mitchell, J. E. Braun, Principles of Heating, Ventilation, and Air Conditioning in Buildings, 1st Edition, Wiley, Hoboken, NJ, 2012.
[44] K. Hinkelman, Y. Yang, W. Zuo, Design methodologies and engineering applications for ecosystem biomimicry: An interdisciplinary review spanning cyber, physical, and cyber-physical systems, Bioinspiration & Biomimetics 18 (2) (2023) 021001. doi:10.1088/1748-3190/acb520.
[45] M. Wetter, W. Zuo, T. S. Nouidui, X. Pang, Modelica Buildings library, Journal of Building Performance Simulation 7 (4) (2014) 253–270. doi:10.1080/19401493.2013.765506.
[46] K. Hinkelman, W. Zuo, BICEPS Modelica library (v0.1.0), https://sites.psu.edu/sbslab/ tools/biceps-library (2022).
[47] A. C. Hindmarsh, R. Serban, D. R. Reynolds, User documentation for CVODE v5.1.0 (SUNDIALS v5.1.0), Tech. rep., Lawrence Livermore National Laboratory (2020).
[48] Dassault Systèmes AB, Dymola User Manual Volume 2 (Dymola 2019 FD01), Tech. Rep. September 2018, Dassault Systèmes AB, Lund, Sweden (2018).
[49] ASHRAE, ANSI/ASHRAE/IES Standard 90.1: Energy Standard for Sites and Buildings Except Low-Rise Residential Buildings, Tech. rep., American Society of Heating, Refrigerating and Air-Conditioning Engineers, Peachtree Corners, GA (2022).
[50] ANSI, ASHRAE, Standard methods of determining, expressing, and comparing building energy performance and greenhouse gas emissions, Standard 105-2014 (2014).
[51] K. Peterson, P. Torcellini, R. Grant, A Common Definition for Zero Energy Buildings, U.S. DOE Report (2015).
[52] B. C. Patten, M. Higashi, Modified cycling index for ecological applications, Ecological Modelling 25 (1984) 69–83. doi:10.1016/0304-3800(84)90033-4.
[53] S. Allesina, R. E. Ulanowicz, Cycling in ecological networks: Finn's index revisited, Computational Biology and Chemistry 28 (3) (2004) 227–233. doi:10.1016/j.compbiolchem.2004.04.002.
[54] B. D. Fath, Quantifying economic and ecological sustainability, Ocean and Coastal Management 108 (2015) 13–19. doi:10.1016/j.ocecoaman.2014.06.020.
[55] S. Kullback, Information theory and statistics, dover Edition, Dover Publications Inc, Gloucester, MA, 1978.
[56] R. W. Rutledge, B. L. Basore, R. J. Mulholland, Ecological stability: An information theory viewpoint, Journal of Theoretical Biology 57 (2) (1976) 355–371. doi:10.1016/0022-5193(76)90007-2.
[57] E. Michaelides, Exergy Analysis for Energy Conversion Systems, 1st Edition, Cambridge University Press, Cambridge, 2021. doi:10.1017/9781108635684.
[58] G. Evola, V. Costanzo, L. Marletta, Exergy analysis of energy systems in buildings, Buildings 8 (12) (2018). doi:10.3390/buildings8120180.
[59] S. Jansen, N. Woudstra, Understanding the exergy of cold: Theory and practical examples, International Journal

of Exergy 7 (6) (2010) 693–713. doi:10.1504/IJEX.2010.035516.
[60] P. Remmen, M. Lauster, M. Mans, M. Fuchs, T. Osterhage, D. Müller, TEASER: an open tool for urban energy modelling of building stocks, Journal of Building Performance Simulation 11 (1) (2018) 84–98. doi:10.1080/19401493.2017.1283539.
[61] VDI, Calculation of transient thermal response of rooms and buildings: Modelling of rooms, Tech. Rep. June, German Association of Engineers, Düsseldorf (2015).
[62] M. Hydeman, K. L. Gillespie, A. L. Dexter, Tools and techniques to calibrate electric chiller component models, ASHRAE Transactions 108 PART 1 (2002) 733–741.
[63] M. Wetter, Fan and Pump Model that has a Unique Solution for any Pressure Boundary Condition and Control Signal, in: The 13th Conference of International Building Performance Simulation Association, Chambéry, France, 2013, pp. 3505–3512.
[64] United States Department of Energy, EnergyPlus Version 8.9.0 Documentation: Engineering Reference, Tech. rep., U.S. DOE (2018).
[65] T. Sommer, M. Sulzer, M. Wetter, A. Sotnikov, S. Mennel, C. Stettler, The reservoir network: A new network topology for district heating and cooling, Energy 199 (2020) 117418. doi:10.1016/j.energy.2020.117418.
[66] M. Wetter, J. Hu, Quayside Energy Systems Analysis, Lawrence Berkeley National Laboratory LBNL-20011 (March) (2019).
[67] B. van der Heijde, M. Fuchs, C. Ribas Tugores, G. Schweiger, K. Sartor, D. Basciotti, D. Müller, C. Nytsch-Geusen, M. Wetter, L. Helsen, Dynamic equation-based thermo-hydraulic pipe model for district heating and cooling systems, Energy Conversion and Management 151 (2017) 158–169. doi:10.1016/j.enconman.2017.08.072.
[68] M. Iyengar, M. David, P. Parida, V. Kamath, B. Kochuparambil, D. Graybill, M. Schultz, M. Gaynes, R. Simons, R. Schmidt, T. Chainer, Server Liquid Cooling with Chiller-less Data Center Design to Enable Significant Energy Savings, in: 28th IEEE SEMI-THERM Symposium, IEEE, 2012.
[69] NREL, High-Performance Computing Data Center Power Usage Effectiveness (2021).
URL https://www.nrel.gov/computational-science/measuring-efficiency-pue.html
[70] Mission Critical, Two-Phase Immersion Cooling Project Uses 3M Novec 7100 Fluid (2015).
URL https://www.missioncriticalmagazine.com
[71] S. Jansen, M. Fremouw, F. Meggers, H. Guo, P.-R. Schmidt, C. Maguerite, I. Martinac, G. Kayo, C. Wang, O. Gudmundsson, M. Brand, K. L. Nielsen, S. Svendsen, M. Harrestrup, X. Yang, C. Sager-Klauss, J. Orozaliev, I. Best, M. Baranski, R. Sangi, S. Saydi, F. Dammel, P.-M. Falk, E. Willems, P. O. Veld, M. G. Baldi, P. Caputo, F. Zagarella, S. Kilkis, LowEx Communities - Optimised Performance of Energy Supply Systems with Exergy Principles (Annex 64), Tech. Rep. September, Fraunhofer Verlag, Stuttgart, Germany (2019).
[72] Edwards, Christopher, Exergy 101, in: CCEP Symposium 2012, Stanford ENERGY, 2012.
URL https://www.youtube.com/watch?v=XgG3LtJqFMw
[73] J. T. Ibarra, K. L. Cockle, T. A. Altamirano, Y. van der Hoek, S. W. Simard, C. Bonacic, K. Martin, Nurturing resilient forest biodiversity: Nest webs as complex adaptive systems, Ecology and Society 25 (2) (2020) 27. doi:10.5751/ES-11590-250227.
[74] C. Duan, B. Chen, K. Feng, Z. Liu, T. Hayat, A. Alsaedi, B. Ahmad, Interregional carbon flows of China, Applied Energy 227 (2018) 342–352. doi:10.1016/j.apenergy.2018.01.028.
[75] D. Fang, B. Chen, Information-based ecological network analysis for carbon emissions, Applied Energy 238 (19) (2019) 45–53. doi:10.1016/j.apenergy.2019.01.066.
[76] Y. Zhang, Y. Li, G. Liu, Y. Hao, CO2 metabolic flow analysis in global trade based on ecological network analysis, Journal of Cleaner Production 170 (2018) 34–41. doi:10.1016/j.jclepro.2017.08.244.
[77] Y. Wang, L. Wang, Z. Li, Dynamic analysis of China's imported raw milk powder consumption, Sustainability 12 (4) (2020) 1542. doi:10.3390/su12041542.
[78] S. Wang, Y. Liu, T. Cao, B. Chen, Inter-country Energy Trade Analysis Based on Ecological Network Analysis, in: Applied Energy Symposium and Forum, CUE2016: Low carbon cities and urban energy systems, Vol. 104, 2016, pp. 580–584. doi:10.1016/j.egypro.2016.12.098.
[79] X. Li, H. Su, J. Zhang, A systematic assessment method of supply resilience for natural gas supply systems, Chemical Engineering Research and Design 182 (2022) 207–215. doi:10.1016/j.cherd.2022.03.057.
[80] L. Xueyi, Z. Jinjun, S. Huai, E. Zio, Resilience Assessment of China's Natural Gas Supply System Based on Ecological Network Analysis, in: The 4th International Conference on System Reliability and Safety, ICSRS 2019, 2019, pp. 402–406. doi:10.1109/ICSRS48664.2019.8987713.
[81] E. Briese, K. Piezer, I. Celik, D. Apul, Ecological network analysis of solar photovoltaic power generation systems, Journal of Cleaner Production 223 (2019) 368–378. doi:10.1016/j.jclepro.2019.03.112.

[82] A. Kharrazi, E. Rovenskaya, B. D. Fath, M. Yarime, S. Kraines, Quantifying the sustainability of economic resource networks: An ecological information-based approach, Ecological Economics 90 (2013) 177–186. doi:10.1016/j.ecolecon.2013.03.018.
[83] A. Layton, B. Bras, M. Weissburg, Ecological Robustness as a Design Principle for Sustainable Industrial Systems, in: ASME 2015 International Design Engineering Technical Conferences & Computers and Information in Engineering Conference (IDETC/CIE), Boston, MA, 2015, pp. 1–8. doi:10.1115/DETC2015-47560.
[84] Z. B. Morris, M. Weissburg, B. Bras, Ecological network analysis of urban-industrial ecosystems, Journal of Industrial Ecology 25 (1) (2021) 193–204. doi:10.1111/jiec.13043.
[85] S. M. Malone, A. R. Cohen, B. Bras, M. Weissburg, The Application of Detrital Actors in Industrial Systems, in: The 25th CIRP Life Cycle Engineering (LCE) Conference, Vol. 69, Copenhagen, Denmark, 2018, pp. 867–871. doi:10.1016/j.procir.2017.11.091.
[86] Z. B. Morris, S. M. Malone, A. R. Cohen, M. J. Weissburg, B. Bras, Impact of Low-Impact Development Technologies from an Ecological Perspective in Different Residential Zones of the City of Atlanta, Georgia, Engineering 4 (2) (2018) 194–199. doi:10.1016/j.eng.2018.03.005.
[87] S. Yang, B. Fath, B. Chen, Ecological network analysis of embodied particulate matter 2.5 – A case study of Beijing, Applied Energy 184 (2016) 882–888. doi:10.1016/j.apenergy.2016.04.087.
[88] Y. Li, Y. Cao, H. Liu, M. Li, B. Xuan, X. Zhang, X. Gao, J. Zhao, Contribution of wastewater treatment engineering measures in cities to reducing NH3–N export to sea from subarea and river network perspectives using ecological network analysis: A case study of Fuzhou, China, Ocean and Coastal Management 236 (2023) 106501. doi:10.1016/j.ocecoaman.2023.106501.
[89] R. Petela, Exergy of heat radiation, Journal of Heat Transfer 86 (2) (1964) 187–192. doi:10.1115/1.3687092.

Appendix

Literature Review

Table 4 summarizes previous literature on ENA for non-biological applications.

Traditional Key Performance Indicators

This section presents the formulations of traditional KPIs used as bases of comparison in this study. For data centers, a common efficiency metrics is the power usage effectiveness PUE, given as on an annualized average basis as

$$PUE = \frac{\int_{t_1}^{t_2} P_{dat}(t,\cdot)\, dt}{\int_{t_1}^{t_2} P_{ser}(t,\cdot)\, dt}, \tag{16}$$

where $P_{dat}(t,\cdot)$ is the instantaneous total power of the data center at time t and $P_{ser}(t,\cdot)$ is the power of the servers only.

For the entire site, energy efficiency η_I can be represented on both site (sit) and source (sou) bases. Because the involved system does not have on-site renewable energy being exported, $\eta_{I,sit}$ and $\eta_{I,sou}$ are

$$\eta_{I,sit} = \frac{\sum_{k\in K} \int_{t_1}^{t_2} P_{out,k}(t,\cdot)\, dt}{E_{sit}} \quad \text{and} \tag{17}$$

$$\eta_{I,sou} = \frac{\sum_{k\in K} \int_{t_1}^{t_2} P_{out,k}(t,\cdot)\, dt}{E_{sou}}, \tag{18}$$

where $P_{out,k}$ is the power delivered to end use outputs for all energy types $k \in K$ (e.g., electricity, natural gas, chilled water, etc.). In these four case studies, P_{out} includes both the electricity

Table 4: Previous case studies adopting ENA for non-biological applications.

Reference(s)	Steady balance	Time step	System use case(s)	ENA unit(s)	Scale
[24]	Yes	1 y	carbon dioxide emissions	mass	district
[74, 75]	Yes	1 y	carbon dioxide emissions	mass	national
[76]	Yes	1 y	carbon dioxide emissions	mass	global
[9]	Yes	1 y	carpet recycling	mass	city metro
[77]	Yes	1 y	dairy market	mass	national
[10]	Yes	1 w	electric motor supply chain *	no. parts	national
[38, 37]	Yes †	design	electric power networks	real power	regional
[11]	Yes	design	cyber-physical power *	real power x packets	regional
[78]	Yes	1 y	energy trade *	N/A	global
[31, 32]	Yes	1 y	energy *	energy	city
[27]	Yes	1 y	energy *	energy	city
[33]	Yes	1 y	energy *	energy	state
[30]	Yes	1 y	energy-water *	energy + volume	multi-regional
[28]	Yes	1 y	energy-water *	energy x volume	multi-regional
[25]	Yes	1 y	embodied energy	energy	national
[36]	No	1 w	forestry industry	mass/capita	regional
[34]	Yes	design	hypothetical network *	task-1+task-2+task-3	N/A
[79]	Yes	1 y	natural gas	volume	national
[80]	Yes	1 y	natural gas *	heating value	national
[81]	Yes	30 y	photovoltaic power	energy	district
[82]	Yes	1 y	trade	currency	global
[83]	Yes	1 y	trade/water/other	currency, volume	regional–global
[84]	Yes	1 y	urban-industrial	mass, energy	district–national
[29]	Yes	1 y	urban-industrial *	energy+mass	city
[85]	Yes	1 y	water in steel industry	volume/mass	district
[86]	Yes	1 y	residential water	volume	city
[26]	Yes	1 y	water	volume	city
[35]	Yes	1 y	water	volume	district
[87]	Yes	1 y	PM 2.5 emissions	mass	city
[88]	Yes	1 y	water pollutants	mass NH_3-N	city

* This study aggregated two or more distinct flow types in single ENA models.
† PowerWorld dynamic flows, steady flows used for long-term planning ENA.

delivered to servers/office equipment and heat added to (extracted from) the zones for heating (cooling). Site energy E_{sit} and source energy E_{sou} are

$$E_{sit} = \sum_{k \in K} \int_{t_1}^{t_2} P_{in,k}(t, \cdot)\, dt \quad \text{and} \tag{19}$$

$$E_{sou} = \sum_{k \in K} r_k \int_{t_1}^{t_2} P_{in,k}(t, \cdot)\, dt, \tag{20}$$

where $P_{in,k}$ is the power input to the site of energy type k and r_k is the source energy conversion factor for energy type k per [51] or [50].

The total number of *unmet hours* by the HVAC system is an indicator of thermal discomfort. The unmet hours t_{unm} is

$$t_{unm} = \sum_{z=1}^{N} \int_{t_1}^{t_2} \left[\max\left(\frac{T_z(t, \cdot) - T_{z,coo}(t)}{T_z(t, \cdot) - T_{z,coo}(t)}, 0 \right) + \max\left(\frac{T_{z,hea}(t) - T_z(t, \cdot)}{T_{z,hea}(t) - T_z(t, \cdot)}, 0 \right) \right] dt, \tag{21}$$

where T_z is the zone temperature, $T_{z,coo}$ is the zone temperature setpoint during cooling, and $T_{z,hea}$ is the zone temperature setpoint during heating.

Network Flows

Table 5 and Table 6 present the equations for network flows and storages adopted in the four case study systems. The *Nomenclature* section includes definitions of all variables, subscripts, and superscripts. For case study redesign 3 (liquid cooling at the data center), the network flows and storages are the same as those presented in Table 6 except for $\dot{f}_{14}$, $\dot{z}_4$, $\dot{y}_4$, and X_4. Instead, these are

$$\dot{f}_{14,redesign3} = P_{aux,Pum} \tag{22}$$

$$\dot{z}_{4,redesign3} = \dot{m}_{datRW} \left| h_{datRW} - h_{OW} - T_{OW}(s_{datRW} - s_{OW}) \right| \tag{23}$$

$$\dot{y}_{4,redesign3} = \dot{m}_{datSW} \left| h_{datSW} - h_{OW} - T_{OW}(s_{datSW} - s_{OW}) \right| \tag{24}$$

$$X_{4,redesign3} = 0 \tag{25}$$

Table 5: Network flows and storages for the baseline case study with separate systems. All flows correspond to edges in Figure 13(a). Only storage equations for compartments with a dynamic exergy balance are shown. See Figure 4 for a visual representation of flow types. All variables, subscripts, and superscripts are defined in the *Nomenclature* section.

	Compartment (Origin if flow)	Destination	Equation
Inter-compartment	Electrical	Office HVAC	$\dot{f}_{12} = P_{offFan} + P_{offHea} + P_{offCoo} + P_{offPum}$
	Electrical	AHU	$\dot{f}_{14} = P_{AHU,Fan} + P_{AHU,Hea}$
	Electrical	Chiller/WSE	$\dot{f}_{15} = \sum_{i=1}^{2} P_{CH,i} + \sum_{i=1}^{2} P_{CHWP,i}$
	Electrical	Cooling tower	$\dot{f}_{16} = \sum_{i=1}^{2} P_{CWP,i} + \sum_{i=1}^{2} P_{CT,i}$
	AHU	Chiller/WSE	$\dot{f}_{45} = \dot{m}_{CHWR} \lvert h_{CHWR} - h_{OW} - T_{OW}(s_{CHWR} - s_{OW}) \rvert$
	Chiller/WSE	AHU	$\dot{f}_{54} = \dot{m}_{CHWS} \lvert h_{CHWS} - h_{OW} - T_{OW}(s_{CHWS} - s_{OW}) \rvert$
	Chiller/WSE	Cooling tower	$\dot{f}_{56} = \dot{m}_{CWR} \lvert h_{CWR} - h_{OW} - T_{OW}(s_{CWR} - s_{OW}) \rvert$
	Cooling tower	Chiller/WSE	$\dot{f}_{65} = \dot{m}_{CWS} \lvert h_{CWS} - h_{OW} - T_{OW}(s_{CWS} - s_{OW}) \rvert$
Inputs	Source energies	Electrical	$\dot{z}_1 = r_{ele} \left(\sum_{i=2}^{6} \dot{f}_{1i} + \dot{y}_1 \right)$
	Office zone	Office HVAC	$\dot{z}_2 = \dot{m}_{offRA} \lvert h_{offRA} - h_{OA} - T_{OA}(s_{offRA} - s_{OA}) \rvert$
	Ambient & office zone †	Office envelope	$\dot{z}_3 = \dot{Q}_{offRad} \left(1 - \frac{T_{OA}}{T^*}\right) + \max(0, \dot{Q}_{intWal}) \left(1 - \frac{T_{OA}}{T_{intWal}}\right) + \max(0, \dot{Q}_{extWal}) \left(1 - \frac{T_{OA}}{T_{extWal}}\right)$
	Server room	AHU	$\dot{z}_4 = \dot{m}_{datRA} \lvert h_{datRA} - h_{OA} - T_{OA}(s_{datRA} - s_{OA}) \rvert$
Outputs	Electrical	Server room & office zone	$\dot{y}_1 = P_{datSer} + P_{offEqu}$
	Office HVAC	Office zone	$\dot{y}_2 = \dot{m}_{offSA} \lvert h_{offSA} - h_{OA} - T_{OA}(s_{offSA} - s_{OA}) \rvert$
	Office envelope	Office zone	$\dot{y}_3 = \min(0, \dot{Q}_{intWal}) \left(1 - \frac{T_{OA}}{T_{intWal}}\right) + \min(0, \dot{Q}_{extWal}) \left(1 - \frac{T_{OA}}{T_{extWal}}\right)$
	AHU	Server room	$\dot{y}_4 = \dot{m}_{datSA} \lvert h_{datSA} - h_{OA} - T_{OA}(s_{datSA} - s_{OA}) \rvert$
Storage	Office HVAC	–	$X_2 = m_{hea} \lvert h_{hea,i} - h_{OA} - T_{OA}(s_{hea,i} - s_{OA}) \rvert$
	Office envelope	–	$X_3 = \Gamma_{intWal} T_{intWal} \left(1 - \frac{T_{OA}}{T_{intWal}}\right) + \Gamma_{extWal} T_{extWal} \left(1 - \frac{T_{OA}}{T_{extWal}}\right)$
	Chiller/WSE	–	$X_5 = \sum_{i=1}^{2} m_{ChiEva,i} \lvert h_{CHWS,i} - h_{OW} - T_{OW}(s_{CHWS,i} - s_{OW}) \rvert + m_{ChiCon,i} \lvert h_{CWR,i} - h_{OW} - T_{OW}(s_{CWR,i} - s_{OW}) \rvert$
	Cooling tower	–	$X_6 = \sum_{i=1}^{2} m_{CT,i} \lvert h_{CWS,i} - h_{OW} - T_{OW}(s_{CWS,i} - s_{OW}) \rvert$

† $T^* = 3/4 T_s$ and $T_s \approx 5770\,\mathrm{K}$, per the commonly-adopted formulations in [89].

Table 6: Network flows and storages for case study redesign 1 and 2. All flows correspond to edges in Figure 13(b). Only storage equations for compartments with a dynamic exergy balance are shown. See Figure 4 for a visual representation of flow types. All variables, subscripts, and superscripts are defined in the *Nomenclature* section.

	Compartment (Origin if flow)	Destination	Equation
Inter-compartment	Electrical	Office HVAC	See $\dot{f}_{12}$ in Table 5
	Electrical	Data center cooling	$\dot{f}_{14} = P_{AHU,Fan} + P_{AHU,Hea} + \sum_{i=1}^{2} P_{CH,i} + \sum_{i=1}^{2} P_{CHWP,i} + \sum_{i=1}^{2} P_{CWP,i} + \sum_{i=1}^{2} P_{CT,i}$
	Electrical	District	$\dot{f}_{15} = P_{DisPum}$
	Electrical	Borefield	$\dot{f}_{16} = P_{BorPum}$
	Office HVAC	District	$\dot{f}_{25} = \dot{m}_{offDWR} \lvert h_{offDWR} - h_{OW} - T_{OW}(s_{offDWR} - s_{OW}) \rvert$
	Data center cooling	District	$\dot{f}_{45} = \dot{m}_{datDWR} \lvert h_{datDWR} - h_{OW} - T_{OW}(s_{datDWR} - s_{OW}) \rvert$
	District	Office HVAC	$\dot{f}_{52} = \dot{m}_{offDWS} \lvert h_{offDWS} - h_{OW} - T_{OW}(s_{offDWS} - s_{OW}) \rvert$
	District	Data center cooling	$\dot{f}_{54} = \dot{m}_{datDWS} \lvert h_{datDWS} - h_{OW} - T_{OW}(s_{datDWS} - s_{OW}) \rvert$
	District	Borefield	$\dot{f}_{56} = \dot{m}_{BorDWS} \lvert h_{BorDWS} - h_{OW} - T_{OW}(s_{BorDWS} - s_{OW}) \rvert$
	Borefield	District	$\dot{f}_{65} = \dot{m}_{BorDWR} \lvert h_{BorDWR} - h_{OW} - T_{OW}(s_{BorDWR} - s_{OW}) \rvert$
Inputs	Source energies	Electrical	See $\dot{z}_1$ in Table 5
	Office zone	Office HVAC	See $\dot{z}_2$ in Table 5
	Ambient & office zone	Office envelope	See $\dot{z}_3$ in Table 5
	Server room	Data center cooling	See $\dot{z}_4$ in Table 5
	Ambient †	Borefield	$\dot{z}_6 = 350 \sum_{i=1}^{20} \max(0, \dot{Q}_{tubSeg,i}) \left(1 - \frac{T_{OA}}{T_{tubSeg,i}}\right)$
Outputs	Electrical	Server room & office zone	See $\dot{y}_1$ in Table 5
	Office HVAC	Office zone	See $\dot{y}_2$ in Table 5
	Office envelope	Office zone	See $\dot{y}_3$ in Table 5
	Data center cooling	Server room	See $\dot{y}_4$ in Table 5
Storage	Office envelope	–	See X_3 in Table 5
	Data center cooling	–	$X_4 = \sum_{i=1}^{2} m_{ChiEva,i} \lvert h_{CHWS,i} - h_{OW} - T_{OW}(s_{CHWS,i} - s_{OW}) \rvert + m_{ChiCon,i} \lvert h_{CWR,i} - h_{OW} - T_{OW}(s_{CWR,i} - s_{OW}) \rvert + \sum_{i=1}^{2} m_{CT,i} \lvert h_{CWS,i} - h_{OW} - T_{OW}(s_{CWS,i} - s_{OW}) \rvert$
	District	–	$X_5 = \sum_i m_{pip,i} x_{pip,i}$
	Borefield	–	$X_6 = 350 m_{bor} \sum_{i=1}^{20} h_{tubSeg,i} - h_{OW} - T_{OW}(s_{tubSeg,i} - s_{OW})$

† Boreholes are discredited vertically in 5 segments and each bore has a double-U shape (4 tubes per vertical segment). This results in 20 tube segments per borehole.